Basilisk Lizard Inspired Methods for Locomotion on Granular and Aquatic Media with Robotic Applications

by

Vidu Jayanetti

A Thesis Presented in Partial Fulfillment
of the Requirement for the Degree
Master of Science

Approved November 2018 by the
Graduate Supervisory Committee:

Hamidreza Marvi, Chair
Heather Emady
Hyunglae Lee

ARIZONA STATE UNIVERSITY

December 2018

ABSTRACT

The Basilisk lizard is known for its agile locomotion capabilities on granular and aquatic media making it an impressive model organism for studying multi-terrain locomotion mechanics. The work presented here is aimed at understanding locomotion characteristics of Basilisk lizards through a systematic series of robotic and animal experiments. In this work, a Basilisk lizard inspired legged robot with bipedal and quadrupedal locomotion capabilities is presented. A series of robot experiments are conducted on dry and wet (saturated) granular media to determine the effects of gait parameters and substrate saturation, on robot velocity and energetics. Gait parameters studied here are stride frequency and stride length. Results of robot experiments are compared with previously obtained animal data. It is observed that for a fixed robot stride frequency, velocity and stride length increase with increasing saturation, confirming the locomotion characteristics of the Basilisk lizard. It is further observed that with increasing saturation level, robot cost of transport decreases. An identical series of robot experiments are performed with quadrupedal gait to determine effects of gait parameters on robot performance. Generally, energetics of bipedal running is observed to be higher than quadrupedal operation. Experimental results also reveal how gait parameters can be varied to achieve different desired velocities depending on the substrate saturation level. In addition to robot experiments on granular media, a series of animal experiments are conducted to determine and characterize strategies exhibited by Basilisk lizards when transitioning from granular to aquatic media.

To Amma and Thaththa

ACKNOWLEDGEMENTS

First I would like to thank my advisor Dr. Hamidreza Marvi for his constant guidance, time and effort. In particular I thank him for introducing me to this path of study. I would like to extend my sincere appreciation to all members of the Bio-Inspired Robotics, Technology and Healthcare Lab (BIRTH Lab) at Arizona State University. In particular, I would like to thank all members of the Fluidized Bed Project Group: Hosain Bagheri, Hailey Burch, Clayton Brenner and Joy Arnold whom without, this work would not have been possible.

TABLE OF CONTENTS

Page

CHAPTER Page

LIST OF TABLES

LIST OF FIGURES

Figure Page

Chapter 1

INTRODUCTION

1.1 Motivation and Overview

The effective use of robotic locomotors for terrestrial applications is predicated upon how well locomotion can be achieved over naturally occurring terrains. These terrains often consist of multiple substrates with varying complexity, topography and rigidity. The existence of such ground formations, each with different properties demand unique locomotion techniques and is a key limitation for many modern terrestrial robots. In contrast, multiple terrestrial animals constantly traverse and navigate complex environments with relative ease. Legged animals in particular have been observed to encounter these natural terrains effectively. These animals can tackle rugged mountain ranges, snowy landscapes, sand dunes and even aquatic environments.

Granular and aquatic substrates in particular are challenging terrains for robotic locomotors. Unlike rigid media, deformability of these substrates cause energy dissipation upon locomotor contact resulting in increased (locomotor) energetic requirements. Furthermore, granular and aquatic substrates are ubiquitous in nature and can often be found adjacent to one another. Numerous legged animals have been observed to exhibit effective locomotor performance in both of these environments. Close investigation of animal morphology and locomotion mechanics can often reveal biological factors contributing to locomotor performance, along with physical principles governing animal-media interaction. Moreover, such animals can provide design inspiration to create "bio-inspired" locomotors capable of effectively traversing deformable terrain.

The integration of bio-inspired concepts in robotics has resulted in the complimentary advancement of both disciplines. Systematically studying the interactions of biological entities with their surrounding environments has led to a better understanding of the associated governing physics and how relevant physical principles can be applied to man-made systems. From a biological perspective this has led to deeper insight on how animals adapt to their environments. In terms of robotics, it has led to the design of novel control methods and mechanisms to create robots and machines capable of effectively interacting with complex natural environments.

Utilizing the above framework, the work presented here applied principles of biology, robotics and physics to determine a biologically inspired approach for robotic locomotion on a subset of granular and aquatic media. The work presented here follows a two-step process of robot and animal experiments. Step 1 presents a study conducted with a bio-inspired robot designed with inspiration stemming from the model organism exhibiting desired locomotor performance on granular media. A series of systematic experiments were carried out using the legged robot to determine the effects of gait parameters on locomotor performance. Results were compared with the performance of the model organism under similar experimental conditions, to create a model for animal locomotion on dry and wet granular media. Step 2 focuses on a series of animal experiments focusing on transitioning from a granular substrate to an aquatic media. Attempts were made to classify the animal's transition strategies, characterize aquatic locomotion methods and observe morphological features of the model organism which aid in aquatic locomotion.

Figure 1.2 shows the overall objectives, work flow and the repetitive nature of bio-inspired research. Animal experiments conducted with the model organism on granular and aquatic media reveal the biomechanics of animal locomotor performance. Based on the discovered physics and animal morphology, a robot is designed or mod-

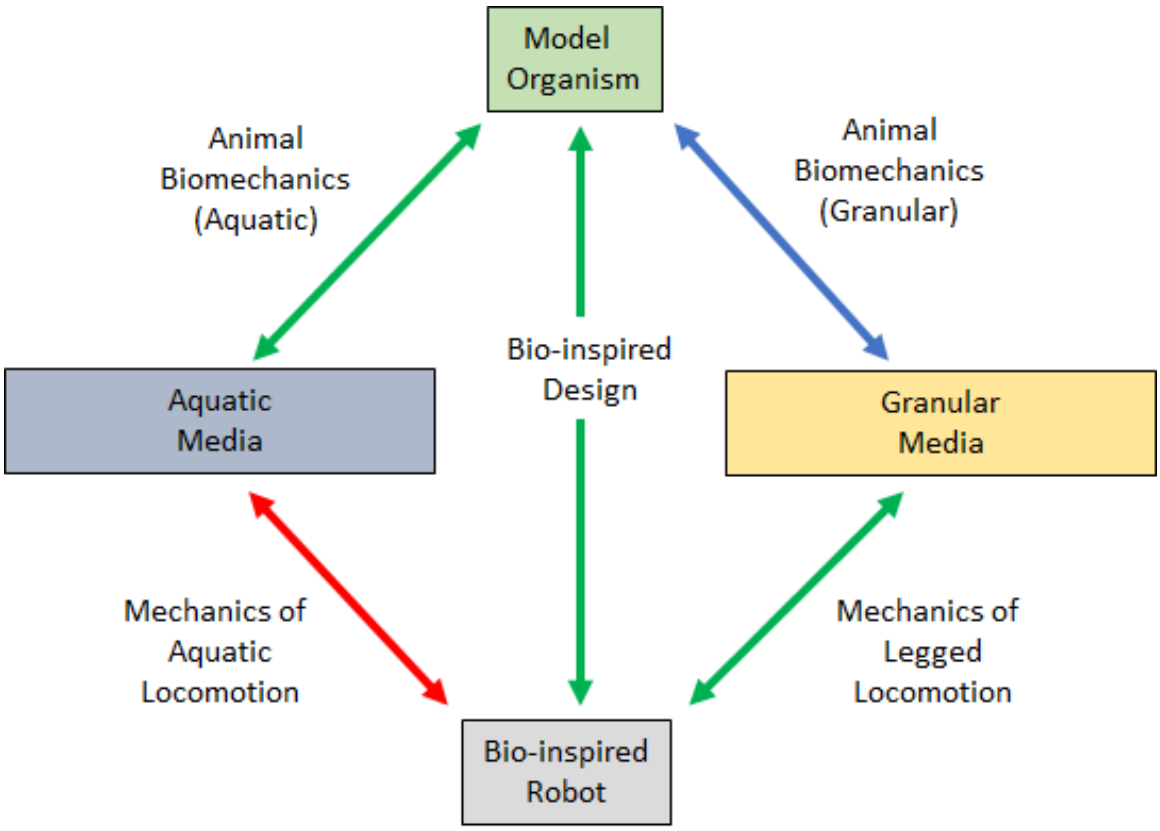

Figure 1.1: Overall scope, objectives and flow of the work presented in the subsequent sections.

ified by way of bio-inspiration. Using the robot in similar substrates allow greater control of gait parameters to determine principles of robotic legged locomotion. Steps highlighted using green arrows depict the work presented in this thesis. Steps given in blue represent studies that have already been conducted while steps depicted in red show future work.

Chapter 1 introduces the model organism used for locomotion studies: the common Basilisk lizard (*Basiliscus basiliscus*), provides a brief background of modern legged robots and their mechanics on granular media, and also introduces standard experimental techniques used for both robot and animal experiments. **Chapter 2** presents BasiliskBot, a Basilisk inspired robot, along with its design and fabrication.

Chapter 3 focuses on bipedal robot experiments conducted on multiple granular substrates to determine the effects of robot gait parameters and substrate properties, on robot performance. Results are compared with previously obtained animal data to draw comparisons with the model organism. **Chapter 4** presents a series of experiments focusing on the robot's quadrupedal performance. **Chapter 5** presents a series of animal experiments conducted with the model organism to determine its transition methods from granular to aquatic media. A brief note on future work and expected outcomes is presented in **Chapter 6**.

1.2 Lizards: A Model Organism for Locomotion Studies

Extensive variation in morphology and locomotor performance over multiple terrains have made lizards an ideal model organism for studying locomotion parameters and gait patterns [1]. The diverse spectrum of lizards hosts many species adept at rapid and efficient locomotion, often evolving from a need to be evasive in the presence of predators, as well as species assuming a slower and more cryptic existence. Species found in similar environments also exhibit drastic differences in both morphology and locomotor performance. For instance, the desert dwelling zebra-tailed lizard (*Callisaurus draconoides*) is known as an agile locomotor where as a desert horned lizard (*Phrynosoma platyrhinos*) is known to be slow and has never been observed to assume a bipedal gait [1].

Depending on morphology, environmental conditions and desired locomotor performance, all lizards commonly employ four symmetric gaits: walking, running-walking, trotting and bipedal running [2]. During quadrupedal gait, the body is supported by diagonally opposite limbs ensuring two points of contact at stance. Unlike most cursorial mammals [3] restricted vertebrae flexion in the saggital plane and limited pelvic movement, forces lizards to engage in a more medio-lateral limb motion, swinging their hind limbs around the body, during swing phase. However, due to limitations in achievable stride length, higher velocities cannot be consistently achieved with a quadrupedal gait and thus the requirement for a bipedal gait resulting in longer stride lengths and higher sprint speeds. Lizards employ reptilian bipedalism, which balances the body over the hind limbs with the tail acting as a cantilever [2].During rapid quadrupedal gait, stride length of the hind limbs and fore limbs are approximately equal to the snout-to-vent length (SVL) while in bipedal running, the stride length can be as three times as long as the SVL[2].

The role played by the tail in locomotor performance depends on a variety of factors including type of lizard species and gait. Experimentally determining the effect of tail on locomotion performance has been made possible by tail autotomy [4],[5] exhibited by many species of lizards. During quadrupedal motion, it has been suggested that the tail can in fact impede performance due to its weight and friction caused by tail-drag [6]. The effect of the tail on bipedal performance is much more direct and bears a strong correlation with sprint speed. Studies performed with Greater Earless Lizards (*Cophosaurus texanus scitulus*) and Colorado Desert Fringe-toed Lizards (*Uma notata notata*) have shown a significant decrease in bipedal sprint speeds in tail-less lizards [7]. *Cophosaurus texanus* showed a 32% decrease in speed and *Uma notata* showed a 42% decrease in speed over a fixed distance. Studies on the Six-lined racerunner (*Cnemidophorus sexlineatus*) has shown a 36% reduction in speed with tail loss [8].

Studies on cursorial mammals have shown metatarsal/femur ratio and hind limb length to be accurate indicators of maximum sprint speed [9]. However, a clear relationship between lizard morphology (particularly hind limb characteristics) and locomotion speed does not exist [1]. It has been suggested that longer limbs allow lizards to take longer stride lengths to achieve higher speeds [10]. Therefore, in theory it can be assumed that it is possible for a lizard with much smaller hind limbs to achieve similar speeds by increasing stride frequency.

1.2.1 Characteristics of the *Basiliscus*

Figure 1.2: An adult Brown Basilisk sitting on a granular surface.

The Common Basilisk (*Basiliscus basiliscus*) is a remarkable class of lizards capable of performing locomotion on multiple terrains and is an ideal model organism for studying locomotor performance. Common Basilisks are decidedly aquatic [11] and can be abundantly found around rivers, streams and lakes in Central and South America. Two types of Basilisk species are studied in this work: the brown Basilisk (*Basiliscus vittatus*) and the green or Plumed Basilisk (*Basiliscus plumifrons*). Adult brown Basilisks can grow to be around 17cm in SVL or $\approx$ 60cm in total length, while females can grow to around 15cm SVL and $\approx$ 55cm in total length [12]. In comparison, green Basilisks can grow to be slightly larger than their brown counterparts: males can grow up to be $\approx$ 75cm [13]. Both species are renowned for being excellent

runners, climbers and swimmers. In addition, they exhibit the unique ability to "run" on the surface of the water. The plumed Basilisk is especially adept at water-running [14].

Walking is performed with a slow quadrupedal gait while higher speeds are achieved by switching to a bipedal gait which heavily utulizes the lizard's hind limbs and tail. An upright bipedal attitude can be accomplished almost instantly from a resting quadrupedal position or a slow-moving quadrupedal gait [15]. Successful bipedalism is ensured by the use of its powerful hind limbs to provide propulsive forces while its long attenuated tail serves as a counterbalance. It has been suggested that the movement of the tail is may even provide forward impetus for the animal [15]. Importance of the tail is evident as it has been observed that through removal of the tail, the Basilisk's bipedalism can be compromised. Studies have shown that for Basilisk lizards with a posterior third of the tail removed, it was either impossible or extremely difficult to maintain a constant bipedal gait for more than two to three strides [15].

Propulsive forces are generated by storing/transmitting energy through its long and powerful hind-limbs. Similar to the Zebra-tailed lizard: another fast runner with similar morphology, hind-limbs of the Basilisk, contains in effect a strut-spring mechanism storing and releasing energy required for forward locomotion [16]. Studies on cursorial mammals have shown metatarsal/femur ratio and hind limb length to be accurate indicators of maximum sprint speed [9]. Similarly, although a clear relationship has not been shown, it has been observed that longer limbs allow lizards to take longer stride lengths to achieve higher speeds [1, 10]. The foot of a Basilsik in particular, accounts for approximately 44% of its hind-limb length [14] and may contribute to their fast running speeds.

The Basilisk's locomotor performance extends beyond rigid surfaces into highly deformable substrates such as water. By preserving a rapid bipedal gait along with

sufficient initial momentum, Basilisks have been observed to transition from land and run at high speeds on the surface of water for small distances [17, 18, 19]. Unlike locomotion on rigid surfaces which allow energy to be stored in limbs, locomotion on deformable surfaces requires extra work to be done by the animal to account for the energy dissipated during the permanent deformation of the media at limb-media interaction [20, 21]. During locomotion on water, the hind limbs act more as force producers as opposed to behaving as strut-spring elements on rigid ground [14]. A complete stride of the hind limb during bipedal running on water is separated into four phases: slap, stroke, recovery-up and recovery down. During slap phase, the lizard rapidly plunges its foot down forcing the displacement of a volume of water. Slap is followed by an upward force producing stroke phase pushing the hind limb further down and backwards, in a medio-lateral motion. A Basilisk's toes contain a series of scales along the length of each digit forming a passive unidirectional series of fringes [12] that expand when the foot is plunged into the water, thus creating greater surface area. During this phase, motion of the foot is followed by an air cavity. Retraction of the foot, or recovery, is then performed by retracting the foot through the air cavity so that drag forces are minimized [14].

Basilisk locomotor performance on water has also been found to be size dependent [22]. Generally, it has been suggested that juvenile Basilisks perform better on water in comparison with adults, as findings have revealed juveniles can generate impulse forces more than twice its bodyweight while adults generated upward force to support only its bodyweight [22]. In addition to bipedal running, Basilisks are excellent swimmers as they have been observed to swim under water for short periods of time to hide from predators [17, 18].

Figure 1.3: Basilisk lizards moving on granular and aquatic media. (Left) An adult female Brown Basilisk (*Basiliscus vittatus*) running on soft unsaturated sand. (Right) A juvenile female Green Basilisk (*Basiliscus plumifrons*) running on water.

1.3 Roboic Platforms for Terrestrial Locomotion

In recent years, several bio-inspired robots have been created for research on robotic legged locomotion. These robots act as physical (artificial) analogues of the biological model organisms from which design inspiration is drawn. Systematic experiments conducted with such artificial locomotors can provide insight into the mechanics of legged locomotion and allow various hypotheses to be tested. Several advantages of bio-inspired robots exist that make locomotion studies simpler. (1) Mechanisms and kinematics of robots are often simpler than the multi degree of freedom (DOF) kinematics of biological organisms and therefore makes the process of analysis simpler. (2) Researchers have greater control over experimental parameters such as gait patterns which are difficult to vary in the case of the animal, as an animal's behavior is governed by physiological and environmental conditions.

A common and extremely useful robotic platform utilized for studying terrestrial locomotion is the popular RHex class of bio-inspired robots [23, 24, 25, 26, 27]. At its simplest level, RHex is a hexapedal robot assuming a dynamically balanced alternating tripod gait inspired by the locomotion of a cockroach [28]. The robot maintains contact with the ground using six compliant C-legs (C-shaped legs) and walking is approximated using the spring loaded inverted pendulum (SLIP) model. Several de-

scendants of the original RHex [24] have achieved better performance over recent years with modified design and control principles. The light-weight hexapod iSprawl [29] can run at 15 body-lengths per second ($2.3ms^{-1}$). SandBot [23] uses a modified clock signal to achieve approximately 1 body lengths per second ($30cms^{-1}$) speed on a granular surface. The bio-inspired Whegs robot, also utilizing a cockroach-like alternating tripod gait, can climb obstacles 175% of its leg height [26].

The performance of SandBot on granular media [23] is of particular interest to the work presented here. An intra-cycle clock signal employing modified fast-swing and slow-stance phases produces effective performance on soft granular terrain and achieves speeds of approximately 1 body lengths per second. The associated leg designs, clock signals and locomotion mechanics combine for a gait pattern termed *rotary walking*. As the work presented in the subsequent sections center around the use of a robotic platform on granular media, it is worth investigating the physics associated with robot leg-media interaction.

1.4 Terradynamics of Rotary Walking

Kinetics of leg-media interaction play a significant role in the performance and energetics of a robot engaged in rotary walking on granular media. Several existing terradynamic principles which have been theoretically and experimentally defined, can be used to capture quantitative information on leg-media interaction. These models take into account characteristics of the granular medium as well as design attributes of the robot. However, many of these models largely focus on dry (unsaturated) granular media and do not adequately investigate the effects of wet (saturated) media. This section briefly discusses existing terradynamic principles and their relevance to the subsequent animal and robot studies.

Volume fraction of the granular medium and leg frequency have been found to

effect velocity of legged robot locomotion on an unsaturated granular medium [23]. Volume fraction (ϕ), defined as the ratio of the true volume of particles in a medium to the total volume occupied by the medium, is indicative of medium yield strength. For unsaturated and loosely packed desert dune sand, $0.586 < \phi < 0.633$ [30]. A previous study [23] has shown that for a fixed leg frequency, robot velocity remains close to zero up to a critical packing factor (ϕ_c) and thereafter increases to an effectively constant value, separating locomotion into two phases termed: swimming and walking (Figure 1.4). For a fixed ϕ, robot velocity increases sub-linearly with increasing leg frequency until a critical leg frequency (ω_c) is reached, after which velocity decreases rapidly to almost zero.

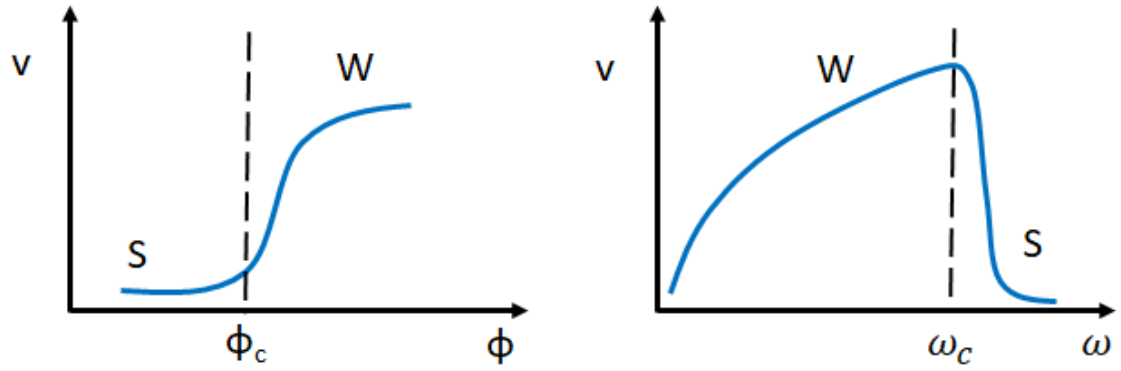

Figure 1.4: A summary of the dependence of volume fraction (ϕ) and leg frequency (ω) on robot velocity (V) in granular media. A critical volume fraction (ϕ_c) and a critical leg frequency (ω_c) separate the locomotion of a legged robot into two phases: swimming (S) and walking (W).

Similar to air and water, dry granular media also exhibit lift and drag forces [31]. A combination of lift and drag forces account for the resistive (and push-off) forces acting on the robot leg and ultimately dictate the performance of legged robot locomotion. Experimental studies [31, 32] have shown that forces in the vertical plane $F_{x,z}$(in horizontal and vertical directions) for an intruder such as a robot leg are proportional to the depth of insertion of the intruder (Equation 1.1). A resistive

force model [32] has shown that the magnitude and direction of resistive forces on simple 2D geometries can be approximated by linear superposition of granular forces on finite elements.

$$F_{x,z} = k(\beta, \gamma)|z| \tag{1.1}$$

Angular leg trajectories of legged robots, particularly the ones introduced in Section 1.3, often employ a slow-stance and fast-swing phase to take advantage of the medium's yielding nature [23, 33]. Initially during stance, the leg rotates slowly with dominant friction forces causing sand behind the leg to yield and compress. As compression reaches a maximum, the sand solidifies and the legs stop further penetration. The legs then start to rotate tangentially on top of the solidified sand and propels the body forward.

The addition of water however, changes the properties of granular media significantly. Limited quantities of water increases the stiffness of sand [34] through capillary cohesion aided by surface tension [35]. Thus, it is evident that the above mentioned models may thereafter lack accuracy to represent the complex interactions of robot legs and wet granular media. Experimental studies [36] however, have shown that for a fixed leg frequency, robot velocity increases with as saturation increases to a certain level. The increased cohesion caused by the addition of water increases push-off force and reduces leg penetration in comparison to dry granular media and may result in increased robot velocity.

1.5 Experimental Techniques

1.5.1 Experimental Setup

Controlled laboratory setups which can accurately recreate natural terrains are highly beneficial towards exploring animal and robotic interactions with granular and

aquatic media. A custom built laboratory test track served as the experimental setup in which both animal and robot experiments were conducted. The setup, referred to in this text as the *transition track* (Figure 1.5), is a 6m long track with 0.5m x 0.5m cross-sectional area. The frame of the structure is assembled using T-slotted Aluminum extrusions (80/20 Inc.) with a cross-sectional area of 1.5" x 1.5".The forward facing wall is lined with transparent acrylic while the remaining walls and bottom are lined with black acrylic sheets with a thickness of 0.5". The top is left open to allow for accessibility. Rubber seals are installed at all acrylic/acrylic interfaces and additional Silicone sealant is applied to all joints to prevent leakage of substrate material. This allows the track to accommodate both solid and liquid media. Up to four mechanical dividers, each constructed with an Aluminum structure and an acrylic wall, can be installed at different locations along the track to separate the inside of the track up to a maximum of five sections. The aim of segmenting the track is to recreate a series of multiple experimental substrates. Type and placement of dividers, varies with the type of experiment conducted and is discussed in further detail in subsequent sections. Sand with particle size ranging from 250 to 600μm was used to create the granular substrate while utility-provided fresh water was used to create the aquatic environment.

1.5.2 Motion Capturing Methods

An Optitrack Infrared(IR) motion capturing system (NaturalPoint Inc.), is utilized to track robot and animal trajectories along the track during each experimental trial. Motion capturing is particularly beneficial in determining animal body position and orientation. The user-friendly nature of the system coupled with its reasonably accurate reconstruction features make this system a viable option for determining locomotor motion. The system described here consists of six OptiTrack Flex 13 cam-

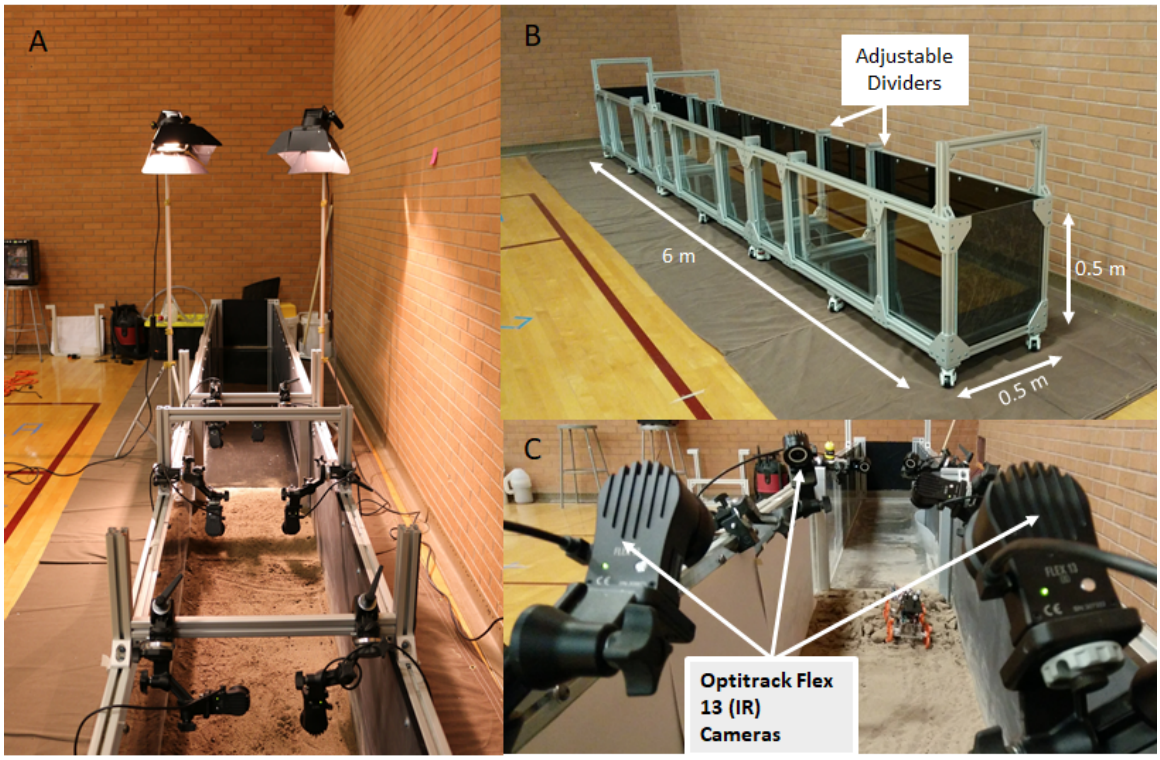

Figure 1.5: The experimental setup utilized for animal and robot studies. (A) A typical experimental setup and surrounding laboratory environment. (B) Physical dimensions of the transition track are shown along with the adjustable mechanical dividers, (C) Optitrack Flex 13 Infrared(IR) cameras mounted above the track is used to track robot/animal motion.

eras, each mounted on a 3-axis tripod head (Manfrotto). The camera and tripod fixtures are mounted on the top rim of the transition track as shown in Figure 1.5(C) and oriented to capture the experimental substrate and maximize image overlap. The system employs a passive marker tracking method in which emitted IR rays are reflected of passive markers attached to either the robot or animal and is recaptured by the camera to determine temporal marker coordinates with respect to a system-defined reference frame. All cameras are connected to a computer by an Optihub 2 USB interface (NaturalPoint Inc.). Motive 1.10.3: OptiTrack's commercial software, serves as the graphical user interface (GUI) to interact with the camera system and provides basic reconstruction and post-processing capabilities. Further data analysis

is performed in a MATLAB R2016a (MathWorks) environment on data sets extracted from Motive 1.10.3.

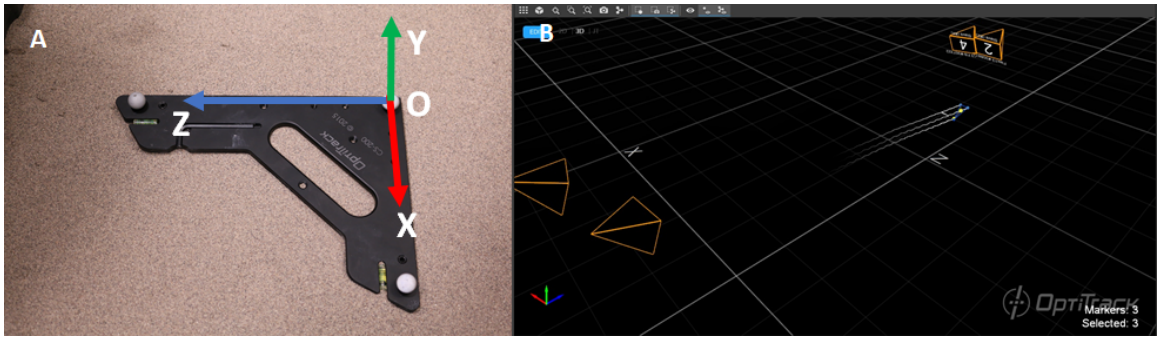

Figure 1.6: Motion capturing method for robot and animal tracking. (A) CS-200 calibration object is used to create a system defined coordinate frame. (B) A screen-capture of Optitrack/Motive 1.10.3 tracking the motion of the robot using four IR cameras. Reference frame corresponding to the calibration square is shown in the bottom left corner.

Chapter 2

BASILISKBOT 2.0: A BASILISK LIZARD INSPIRED ROBOT

2.1 Overview

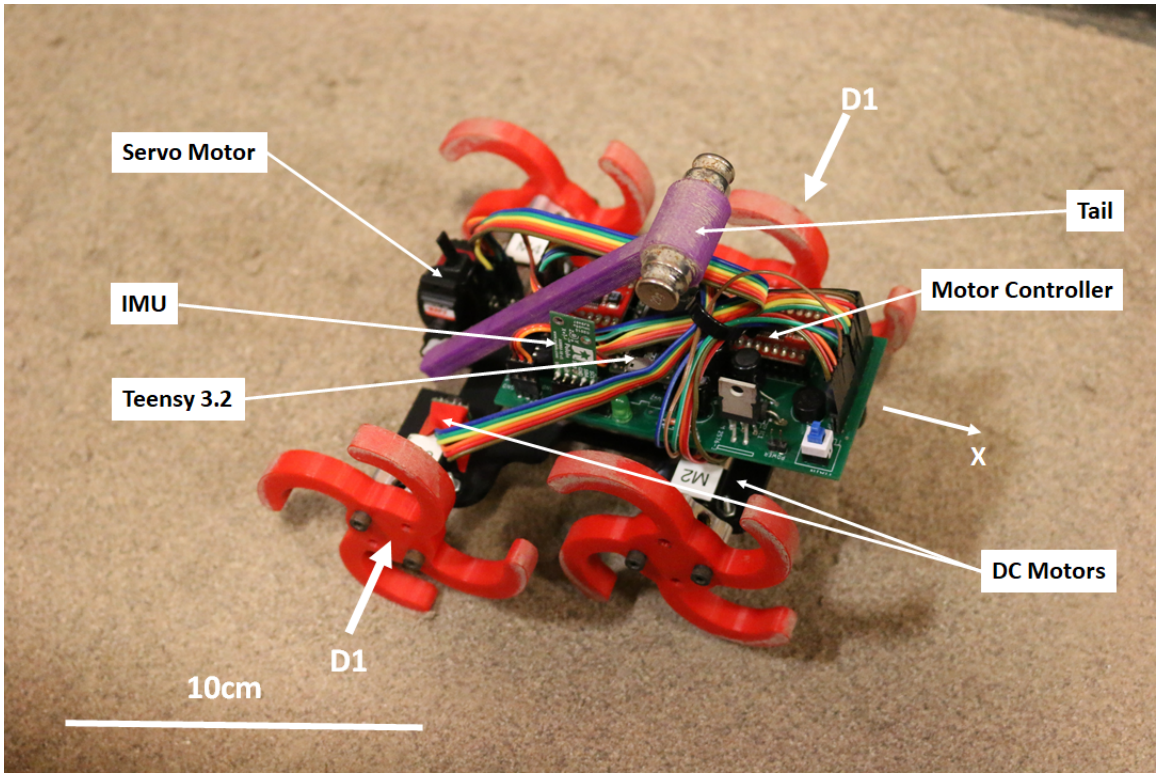

Figure 2.1: BasiliskBot 2.0: a bio-inspired legged robot capable of quadrupedal and bipedal locomotion.

BasiliskBot is a quadruped legged robot designed and built with inspiration stemming from the simplified morphology of the common Basilisk lizard. Similar to the Basilisk's physical makeup, the robot has four actuated limbs and an actuated tail. Limbs are used to interact with the test substrate while the tail serves as a counterbalance enabling bipedal robot locomotion. The test robot was utilized to investigate

the effects of gait parameters on locomotion performance. Use of such a robot allowed precise control of gait parameters over a wide operating range. This chapter describes in detail the following: (1) design and fabrication of the robot, (2) simplified gait control and (3) effective gait parameters relevant to the experimental studies given in Chapters 3 and 4.

2.2 Design and Fabrication

Design of BasiliskBot 2.0 follows an approximation of the physical characteristics of the common Basilisk lizard. The robot is fabricated with a combination of off-the-shelf commercial electronic components, and lightweight structural components produced using rapid prototyping techniques. Rigid whegs [35]: a combination of legs arranged in the form of a wheel, act as the robot's limbs and is used to interact with the environment.

Base measurements for robot whegs and tail were obtained by averaging forelimb, hindlimb and tail length of three Basilisk lizard subjects. The resulting measurements for forelimbs (FL)= 3.05 ± 0.25cm, hindlimbs (HL)= 6.63 ± 0.44cm and tail (T)= 17 ± 2.89cm were subsequently used to design robot whegs and tail. For design simplicity, all robot limbs were designed to be of equal dimensions. The average of animal forelimb and hindlimb length was used as the effective robot wheg length ($2r_o$). Wheg length or effective hip-contact length of the robot limb is 4.24cm. The resulting animal/robot limb scaling of ≈ 2.5 was maintained by creating a robot tail 12.5cm in length. A detailed model of the robot and design parameters used can be seen in Figure 2.2.

Modular design of the robot allowed the attachment of multiple wheg geometries. Each robotic wheg consisted of multiple angularly arranged C-shaped elements. Different wheg geometries were accomplished by varying the number of C-elements in

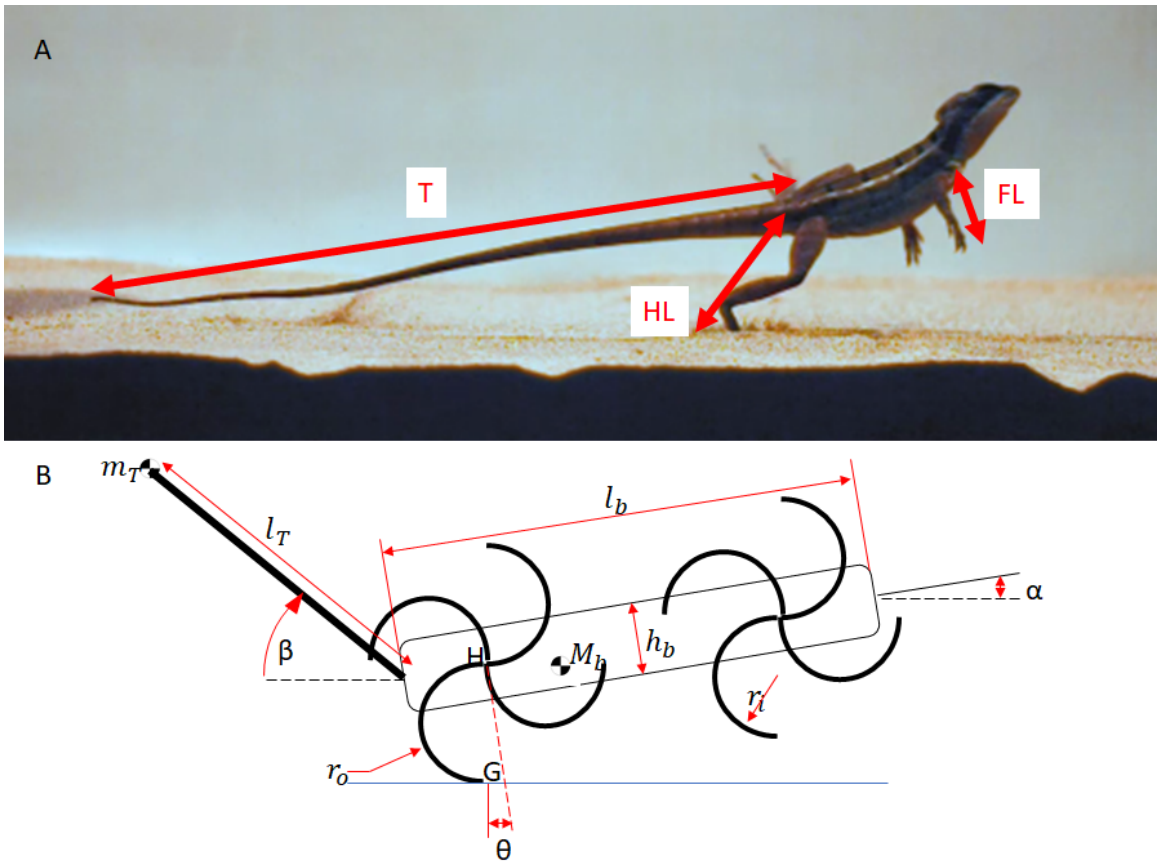

Figure 2.2: Physical comparison between a brown Basilisk(A) and BasiliskBot(B). Robot limb and tail length is scaled based on the corresponding measurements of the model organism. Effective robot limb length, i.e. hip-ground length $(2r_o) = \frac{HL+FL}{2}$ and robot tail $(l_T) = \frac{2r_o * T}{HL}$. Body length (l_b), body height (h_b) and body width (w_b) are independent design parameters defined based on design requirements and practical reasons.

a wheg and thus changing the effective stride length. For the purposes of this work, 5 different wheg geometries, were prototyped using a 3D printer with Acrylonitrile Butadiene Styrene (ABS) as the prototyping material. The wheg geometries were termed L3, L4, L5, L6 and L7, based on the number of C-elements used. The following 3D printing parameters: (1) percentage infill, (2) shell thickness and (3) number of layers per shell were varied per each set of whegs to achieve a mean wheg weight of 10g and thus ensure a constant overall robot weight. Permissible calculation errors

Wheg	M (g)	ϕ (deg)
L3	9.27	120
L4	10.36	90
L5	10.17	72
L6	9.57	60
L7	10.58	51

Table 2.1: Weight (M) and angle between consecutive C-elements (ϕ) of experimental whegs

	Parameters	Symbol	Value	Units
Body	Body Length	l_b	141.5	mm
	Body Width	w_b	96.0	mm
	Body Height	h_b	65.2	mm
	Body Mass	M_b	285.5	g
Legs	Leg Radius(Outer)	r_o	21.4	mm
	Leg Radius(Inner)	r_i	14.0	mm
	Leg Mass	m_l	10.0	g
Tail	Tail Length	l_T	125.0	mm
	Tail Mass	m_T	46.0	g

Table 2.2: Key physical parameters of BasiliskBot.

and limitations in prototyping methods resulted in a mean wheg weight of 9.99g and standard deviation of 0.55g. Several key physical parameters of each set of whegs are denoted in Table 2.1. In addition to variability of effective stride length, the use of multiple C-elements reduced angular speed requirements of the driving motors [27].

Each wheg is actuated by a 12V High-Power Carbon Brush (HPCB) Micro Metal Gearmotor (Pololu) with gear ratio 51.45:1 (50:1). The gearbox of each motor contains a D-cut output shaft 9mm in length and 3mm in diameter. Each wheg is coupled

to its corresponding DC motor shaft by a universal Aluminum mounting hub (Pololu) with an internal diameter of 3mm and secured to the motor shaft by set screws. The wheg-motor assembly is mounted to the 4mm thick Acrylic robot base with plastic mounting brackets and metal screws. The 12.5cm long rigid tail assembly comprises of a 3D printed ABS tail and two additional calibrated weights each weighing 20g attached to the distal end of the tail. The near end of the tail is connected to and directly actuated by a 6V Power HD-1810 Metal Gear DC servo motor mounted to the robot base.

Processing and execution of control algorithms is done by a commercially available Teensy 3.2 32-bit Arduino-compatible micro-controller (PJRC Electronics) powered by a 72MHz Cortex M4 processor. The Teensy's size and high number of multipurpose input and output (I/O) ports made it physically and functionally compatible for the purpose of controlling a robot of such size. Two SparkFun TB6612FNG-1A (SparkFun Electronics) dual motor drivers are used to control all four DC motors actuating the whegs, with one driver actuating the front pair of DC motors and the other, the rear. Angular position and velocity of whegs are measured using magnetic quardrature encoders with a resolution of 12 counts per revolution (CPR) of motor shaft, i.e. 600 CPR of the motor-gearbox output shaft. Each encoder unit comprises of a dual-channel Hall effect sensor board and a 6-pole magnetic disc. The extended back shaft of the DC motor allows for a tight fit between the magnetic disc and the shaft.

An AltIMU-10 V5 (Pololu) Inertial Measurement Unit (IMU), mounted to the body of the robot is used to determine its orientation with respect to the ground. The IMU features a LSM6DS33 gyroscope and accelerometer and LIS3MDL magnetometer. Sensitivities of the gyroscope and accelerometer are $\pm 2000 deg/s$ and $\pm 16g$ respectively.

The 3.3V operating voltage required for the Teensy 3.2 controller, Sparkfun dual

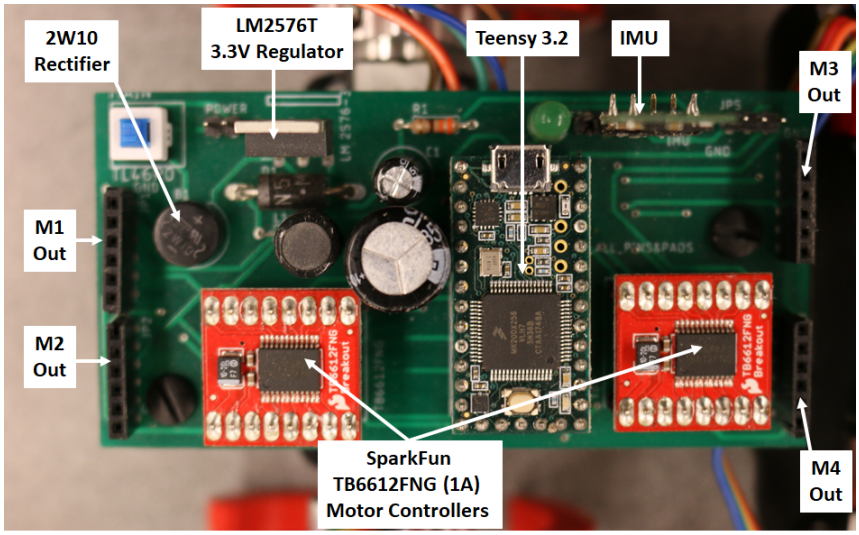

Figure 2.3: The on-board robot controller, motor controllers and power regulating circuitry.

motor drivers and the Pololu AltIMU-10 V5 IMU is supplied by a LM2576T (Texas Instruments) switching voltage regulator circuit. Reversed polarity protection is ensured by a 2W10 bridge rectifier (Multicomp). All electronic components are mounted on a printed circuit board (PCB) with dimensions 5cm x 10cm, designed using Autodesk Eagle CAD. The designed PCB is a 1.6mm thick two-layer fiberglass-reinforced (FR-4) board with a hot-air-solder-leveling (HASL) finish. The scale of the robot as well as design requirements do not permit an on board power supply.The robot is therefore tethered and powered by an external power source. The figure below shows schematic diagram for the electronic circuitry of the robot.

2.3 Robot Gait Control

A closed-loop DC motor controller for quadrupedal motion achieves target trajectories for alternating diagonals D1 and D2 (Figure 2.4). The following two variables are given as the control parameters: initial wheg phase (ϕ) and motor speed (ω). Prior to motion, a closed-loop motor position controller offsets D1 and D2 by an angle of ϕ unique to each wheg geometry. Initial wheg phase is defined by $\phi = \frac{\pi}{n}$, where n is the number of C-legs in a particular wheg. In one cycle both diagonals rotate 2π radians with a constant angular velocity of ω and a time-period of $t = \frac{2\pi}{\omega}$. The robot employs the same alternating diagonal gait to achieve bipedal motion with actuation of only the rear motors (M3 and M4).

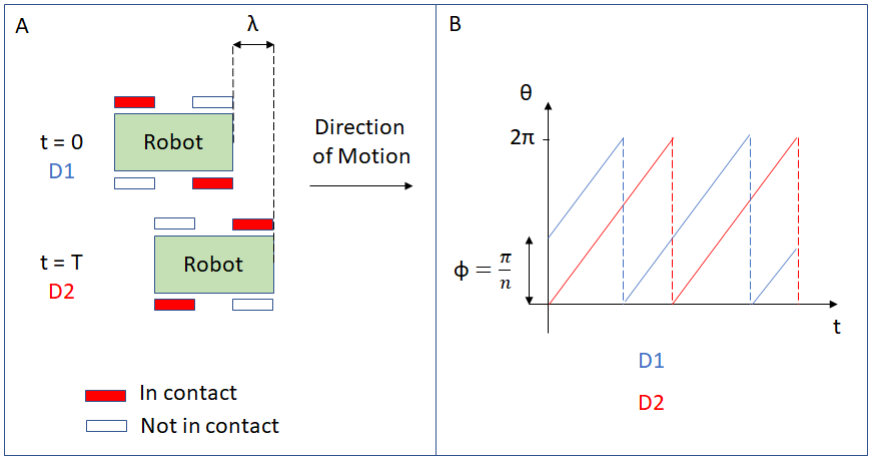

Figure 2.4: Leg trajectories and gait control parameters of BasiliskBot. Two diagonals D1 and D2 alternate to produce a quadrupedal gait. The gait control parameters are motor speed (ω) and wheg offset (ϕ).

A simple proportional-derivative (PD) controller was used to control motor position and motor speed. Application of Newton's law (Equation 2.1) and Kirchoff's voltage law (Equation 2.2) and subsequent application of Laplace transforms produced the transfer function (Equation 2.5) relating rotor position θ and input voltage V. Motor torque constant (K) was calculated using technical specifications of the DC

motor. For the 12V Pololu DC motor, K was calculated to be $0.1NmA^{-1}$. For simplification of calculations, it was assumed that back emf constant $K_e = K$. Armature resistance (R) was found by measuring the resistance between positive and negative ports of the Pololu DC motor using a multimeter. Average armature resistance was found to be 13.7Ω based on measurements obtained from four 12V Pololu 50:1 DC motors.

$$J\ddot{\theta} + b\dot{\theta} = Ki \tag{2.1}$$

$$L\frac{di}{dt} + Ri = V - K\dot{\theta} \tag{2.2}$$

$$Js^2\theta(s) + bs\theta(s) = KI(s) \tag{2.3}$$

$$LsI(s) + RI(s) = V(s) - Ks\theta(s) \tag{2.4}$$

$$\frac{\theta(s)}{V(s)} = \frac{K}{s[(sJ+b)(sL+R)+K^2]} \tag{2.5}$$

$$\frac{\dot{\theta}(s)}{V(s)} = \frac{K}{(sJ+b)(sL+R)+K^2} \tag{2.6}$$

$$C = K_p + \frac{K_i}{s} + K_d s \tag{2.7}$$

The transfer functions were modeled in MATLAB to determine appropriate base values for controller gains. Subsequent tuning of gains were performed experimentally. In the case of motor position control, the desired position in degrees was given as the reference input. The dual channel magnetic encoders attached to the DC motors provided 12 CPR of the motor shaft and thus, 600 CPR (12x50) of the gearbox output shaft, provided angular position of the motor shaft. The above controller was implemented in the Teensy 3.2 micro-controller to provide a constant offset between diagonals D1 and D2. The implemented control algorithm utilized Motor 4 (M4) as its reference motor to read motor position and speed. All other motor positions were synchronized based on M4.

The following simple PID controller with experimentally determined gains K_p, K_i and K_d, was implemented during bipedal motion to control the tail servo and maintain an effectively constant body orientation.

$$\beta_i = K_P * e_i + K_i * (I + e_i * dt) + K_d * (\frac{e_i - e_{i-1}}{dt}) \tag{2.8}$$

Where β_i is the current tail angle correction, e_i is the current robot pitch error, e_{i-1} is previous robot pitch error and dt is sampling time.

Chapter 3

BIPEDAL LOCOMOTION ON DRY AND WET GRANULAR MEDIA

3.1 Overview

Briefly revisiting a previously conducted series of animal experiments [36] show that while stride frequency remains relatively constant over 0%,15% and 30% saturation, stride length and velocity undergoes a statistically significant increase between 0% and 15% and an increase to a lesser degree between 15% and 30%. This can be mostly attributed to higher sinkage of the animal's foot on dry sand and the presence of aerial phase on wet sand. Qualitatively these results can be seen upon close observation of high-speed recordings of an adult female Brown Basilisk running on 0% and 30% saturated sand (Figure 3.1). The time period per stride roughly remains around 200ms at both saturation levels, resulting in an approximate stride frequency of 5Hz. However, a clear increase in stride length can be observed for 30% saturated sand. To verify these results using robotic means, a series of systematic experiments were conducted under similar experimental conditions.

3.2 Robot Experiments

Robot experiments were conducted by repeatedly running the robot along a straight path inside the transition test track introduced in Chapter 1. A mechanical divider was setup inside the transition track to create a 2m long section to accommodate the granular substrate. Four Optitrack Flex 13 IR motion capturing cameras mounted at each corner of the test area were utilized to record kinematics of the robot. Reflective IR markers were attached to the robot which was then repeatedly run on the test sur-

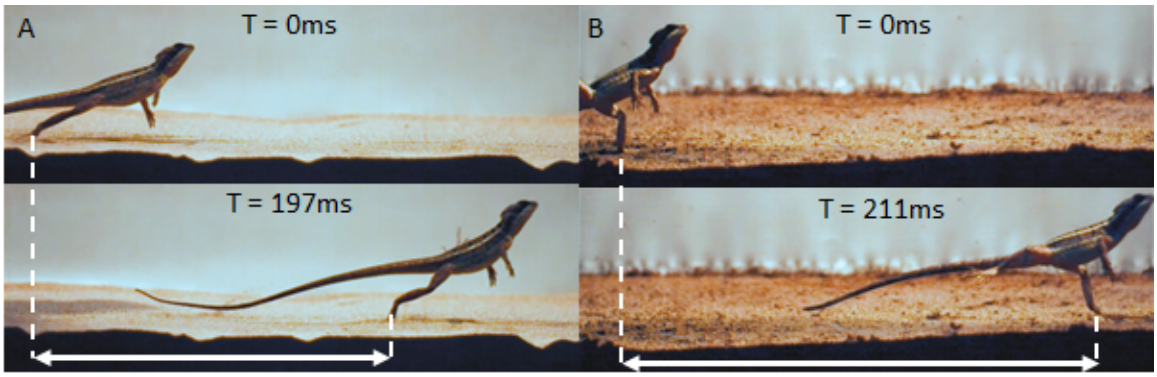

Figure 3.1: Still frames corresponding to a brown Basilisk's stride on dry and wet sand. (A)Brown basilisk running on dry sand with a time period of 197ms. (B)Brown basilisk bipedal running on 30% saturated sand with a time period of 211ms. While stride frequency remained relatively constant, stride length increased significantly.

face while the IR cameras tracked the robot's trajectory inside the track. In tandem with IR motion capturing, representative high-speed videos of each trial were taken from a side-on angle using an Edgertronic SC1 high-speed camera.The tracking data extracted from motion capturing methods and were then analyzed to determine the robot's trajectory and steady-state velocity for each test scenario. High-speed videos provided qualitative information.

3.2.1 Test Track Preparation

Dry Sand

53kg of sieved dry sand with particle sizes ranging from 250μm to 600μm was used to create the medium on which the robot traversed. Once the sand was poured into the experimental setup and evenly distributed. Special attention was given to evening out the sand before and after each run in order to minimize the effects of surface undulations on the robot's movements.

Wet Sand

Measured quantities of water were added to the sand to achieve saturation levels of 15% and 30%. Upon adding necessary amounts of water, the sand was thoroughly mixed with a hand-held sand mixer for even distribution of water along the sand track. Moisture content was measured using a GS1 soil moisture sensor (Decagon Devices) at 10 evenly distributed locations in the sand. The sensor was connected to a computer using a USB6002 (National Instruments) USB interfacing device. A LabView virtual instrument(VI) was used to convert sensor voltage values to readable saturation (%) values. Small amounts of sand was removed by hand to create a small hole in which the sensor was placed such that both probes of the sensor were fully inserted into the side wall of the hole. The hole was then re-filled with previously removed sand and moderately compressed by hand to ensure a compact fit around the probes of the sensor. Saturation readings were then recorded using the LabView VI. The process was repeated for the remaining 9 evenly distributed locations in the sand and averaged to determine the mean saturation level (μ_s). The mixing and measuring process was repeated until the desired saturation level was achieved. For all saturated trials, mean saturation level for a target of 15% was 15.7% resulting in an error of 4.67% while for a target of 30% it was 30.7% resulting in an error of 2.33%. As with dry sand special care was taken to even out the sand before and after each run to minimize surface effects on robot performance.

Camera Calibration

A Micron Series CWM-250 calibration wand and a CS-200 calibration square (Natural Point Inc.) were used to calibrate the set up. Due to the internal dimensions of the transition track, wanding i.e. calibrating, was done by making long sweeping back-

and-forth movements along the XY plane of the test track and ultimately working in the positive Z axis, to cover the entire capture volume. The ground plane was then set using a CS-200 Calibration Square to provide the origin and inertial frame of reference. Optitrack's Motive 1.10.3 Optical Motion Capturing Software was used to record tracking data. Camera settings such as exposure, IR intensity and threshold were determined experimentally to minimize noise generated by sand's natural reflectivity. The experimental setup was housed in a laboratory with an ambient temperature of 78.4^oC and saw minimal variation throughout the entire experimental process. Thus for each experimental session, calibration errors due to temperature variations were assumed to be negligible.

In tandem with IR motion capturing, high-speed video recording was performed to record the performance of the robot. This was done to obtain representative slow-motion videos of each trial and therefore obtain qualitative information. These qualitative information included but were not limited to visual information on (1) the interaction between robot legs and granular media, (2) the effect of different saturation levels on the performance of the legs and (3) the overall motion of the robot body, i.e. roll, pitch and tail movements. To record these high-speed images, an Edgertronic SC1-701FPS @ 720p high-speed color camera was used. The camera features an IR filter with 400-675nm response, 8GB internal memory and a Nikon 50mm f1.8D lens. For all videos the following camera settings were used: a shutter speed of 1/1000s, a frame rate of 500FPS and an aperture setting of 1.8. To provide sufficient levels of lighting required for high-speed imaging, additional lighting was provided using two Lowel DP Tungsten Filament Lamps.

3.2.2 Experimental Process & Data Collection

Kinematic data of the robot: robot position and velocity, were obtained by repeatedly running the robot on sand under different operating conditions and tracking the corresponding robot markers. At each single saturation level (0%, 15% and 30%), the robot was run at 8 different motor frequencies with 3 trials for each frequency. The process was repeated for every wheg geometry (L3-L7), resulting in 120 trials per saturation level. A single representative high-speed recording was performed for each motor frequency per wheg geometry and saturation, resulting in 40 high-speed videos per saturation level.

During bipedal robot locomotion, initially the offset of diagonals D1 and D2 occur between opposing rear whegs: M3 and M4. Once the offset occurred the robot was set down and supported by hand to maintain its initial balance. Although the robot is dynamically balanced during bipedal motion, prior to motion (due to being supported only by a single point of contact) it is not statically balanced and must be supported by hand to maintain its initial balance. Once the robot moved from the near end of the track to the far end resulting in a complete trial, the effective stride length was measured at three locations along the path of the robot using a Digital Vernier Caliper (Pittsburgh) with a minimum measurement of 0.01mm. Effective stride length was defined as the distance between similar features of adjacent indentations caused by C-elements of the same wheg. Close observation of the indentations showed that during the initial stage of the robot path, as it accelerated from rest to steady-state, the robot produced slightly smaller strides in comparison to that of steady-state. Also, upon visual inspection it was noted that even during steady state, due to the flowable nature of granular media, stride lengths appeared to be inconsistent. Therefore the average of three measurements taken at the beginning, middle and end of the robot

tracks was recorded as the effective stride length corresponding to each experimental condition. This process was repeated two more times and the average stride length of all three trials was determined to be the mean effective stride length (λ) corresponding to a particular experimental condition.

Real-time successful marker data acquisition was verified by visual inspection immediately following the completion of a trial. Using Motive's editing capabilities, each take was replayed to determine successful continuous tracking of markers. A successful trial was ensured by the robot following a straight or relatively straight path inside a rectangular grid bounded by four reflective IR markers attached to the walls. If the above condition was not met, the trial was deemed unsuccessful and repeated until the criteria for success was satisfied.

3.3 Data Analysis

Data analysis pertaining to robot kinematics was done in both Motive 1.10.3 and MATLAB R2016b. Motive was used to visualize robot motion in real-time and to perform basic reconstruction of tracking data while MATLAB was used to perform further post-processing, calculating mean steady state velocity and visualizing final data outputs.

Due to a small capture volume, small size of reflective IR markers used, and the oscillatory motion of the robot, continuous tracking of markers was not consistently assured. Therefore wherever necessary, prior to data analysis in MATLAB, Motive was used to reconstruct(stitch) a continuous robot trajectory in three dimensional space using discrete marker segments. The process of stitching involved using linear, polynomial or pattern based interpolation to connect the gaps between segments of marker data. To limit errors, interpolation was performed on gaps with a maximum gap size of 20 samples. As part of reconstruction, noise and artifacts in the form

of random reflections generated due to the disturbance of sand as well as the reflective plastic cover of the robot were removed while preserving the necessary tracking information.

Following reconstruction, the corresponding tracking data was extracted in the form of an Excel file(.xlsx). Tracking data consisted of frame numbers, time-stamps, x, y and z coordinates of the robot with respect to the Optitrack calibration frame (B). In order to compute xyz coordinates with respect to a user-defined inertial frame given by A (V_A), the xyz tracking data vectors (V_B) obtained through Optitrack was pre-multiplyed by the transformation matrix T relating frames A and B as shown in Equation 3.2.

$$T_B^A = \begin{bmatrix} 0 & 0 & 1 \\ 1 & 0 & 0 \\ 0 & 1 & 0 \end{bmatrix} \tag{3.1}$$

$$V_A = \begin{bmatrix} x_A \\ y_A \\ z_A \end{bmatrix} = T_B^A * \begin{bmatrix} x_B \\ y_B \\ z_B \end{bmatrix} \tag{3.2}$$

For the purposes of simplified robot velocity analysis, the velocity of the robot in the XY plane was considered as forward robot velocity (V) while changes in the Z-direction was neglected. The following methodology was used to calculate the XY planar velocity of the robot.

$$\Delta v = \frac{\Delta d}{\Delta t} \tag{3.3}$$

$$v_{i+1} = \frac{\sqrt{(x_{i+1} - x_i)^2 + (y_{i+1} - y_i)^2}}{t_{i+1} - t_i} \tag{3.4}$$

$$y[i] = \frac{1}{N} * \sum_{j=0}^{N-1} x(i+j) \tag{3.5}$$

Given x_i and y_i, x and y positions of the robot at time t_i, and x_{i+1} and y_{i+1}, x and y position of the robot at time t_{i+1}, the instantaneous robot velocity at t_{i+1} was calculated using Equation 3.4. Repetitive application of the above sequence of calculations performed in a MATLAB environment, resulted in XY planar velocities of the robot for each trial. Filtering of the obtained data was done using a moving average filter defined by Equation 3.5 with a window size (n) of 49 samples.

Cycle averaged stride frequencies (f) of BasiliskBot were used to compare the performance of the robot with the *Basiliscus* model organism. Stride frequency, given by units of Hz, was theoretically defined by equations 3.6 and 3.7. Given motor speed (ω) in revolutions per minute and wheg number (L = 3,4,5,6,7), theoretical stride frequency was calculated using equation 3.6. For the same motor speed, multiple stride frequencies can be achieved by attaching multiple wheg geometries.

$$f_1 = \omega * \frac{L}{60} \tag{3.6}$$

$$f_2 = \frac{1}{T} \tag{3.7}$$

However, analysis of high-speed videos obtained using the SC1 camera showed different values for stride frequencies. Enabled by video analysis software (Kinovea), time-stamps of adjacent contacts were averaged to obtain the average time period per contact (T) and stride frequency f_2 using Equation 3.7. The discrepancy was attributed to complex loading patterns of the granular substrate. Frequencies obtained using high-speed video analysis were thus used as the cycle averaged stride frequencies (f).

The final portion of robot data analysis consisted of evaluating mass specific cost

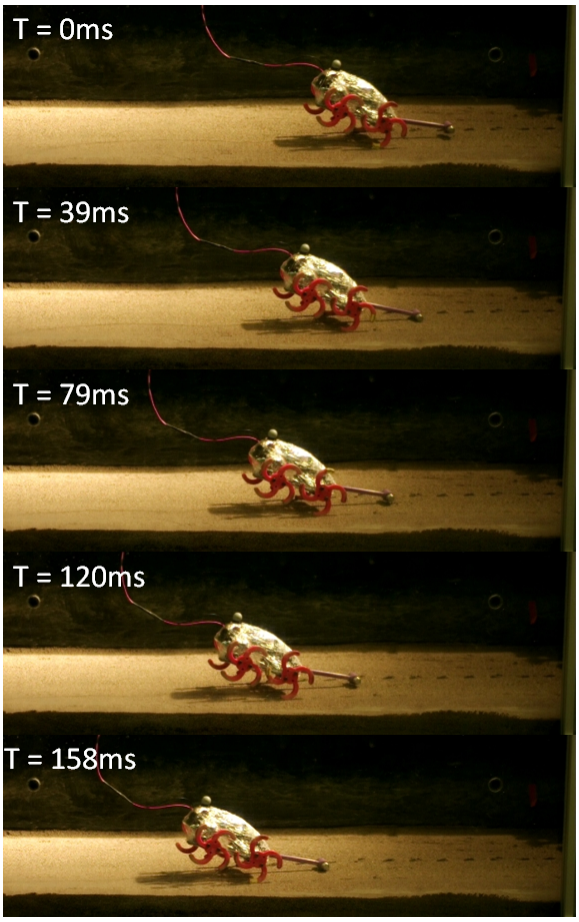

Figure 3.2: BasiliskBot bipedal running at a cycle-averaged stride frequency of ≈25Hz on 30% saturated sand. High-speed video analysis methods were used to determine the time-stamp of each stride and hence the average time period per stride.

of transport for the robot, over the medium under different saturation levels. Cost of transport, defined by Equation 3.9, functioned as the metric used to determine energetics associated with robot locomotion under varying experimental conditions. Power consumption of the robot was calculated using Equation 3.8, where v is the fixed operating voltage of the robot and i is the current drawn by the robot during operation, which was recorded via the tethered power supply. Variables m, g and V are respectively: robot mass, acceleration due to gravity, and steady-state robot

velocity.

$$P = vi \tag{3.8}$$

$$C.O.T. = \frac{P}{mgV} \tag{3.9}$$

3.4 Results

Utilizing the data analysis methods described in Section 3.3, multiple plots were created to visualize the interdependence of effective stride length (λ), cycle averaged stride frequency(f), forward robot velocity (V) and mechanical cost of transport (COT) as it pertains to multiple leg geometries and saturation levels.

Figure 3.3 shows the change of effective stride length with varying stride frequencies for all wheg geometries (L3-L7) under 0%, 15% and 30% saturation levels for bipedal robot motion. Several different conclusions can be made from close observation of the resulting plot. (1) stride length increased with decreasing wheg number, i.e. number of C-elements. (2) At 0% saturation (dry sand), stride length decreased as stride frequency increased. (3) At 15% and 30% saturation levels, a general trend of increasing stride lengths can be observed as stride frequency increases. This increase is more evident for lower wheg numbers (L3 and L4) while for the remaining wheg geometries (L5-L7) the increase is more gradual or relatively constant. (4) Stride length for all wheg geometries increased as saturation level changed from 0% to 15% but remained relatively similar as saturation changed from 15% to 30%. As expected, the first observation becomes obvious as different rigid wheg geometries would result in different stride-lengths. L3 which featured spokes spread out further apart resulted in longer stride lengths while L7, featuring shorter gaps resulted in much smaller stride lengths. The trend of decreasing stride length with increasing stride frequencies on dry sand can be attributed to wheg sinkage, and slippage between whegs and sand. Sinkage occurs when the force exerted by whegs at each point of contact exceeds the

yield strength of the sand. Slippage occurs when whegs spin in place in loose dry sand, impeding robot velocity and forward motion. The third observation can be attributed to aerial phase, which was verified by inspecting representative high-speed videos. On dry sand, the distributed contact load exerted by lower wheg numbers (i.e.L3) on the medium is higher in comparison with distributed contact loads exerted by higher wheg numbers (i.e.L7). Although a single point of contact is desired at each stance phase during robot locomotion, due to the natural sinkage in dry sand, higher wheg numbers can achieve multiple points of contact resulting in a reduction of contact force per C-element. The opposite holds for lower wheg numbers as wider gaps between C-elements prohibits the occurrence of multiple contact points resulting in higher concentrated contact forces. As the weight of the robot is balanced by ground reaction forces at the wheg-sand interface, it can be assumed that for lower wheg numbers, the ground reaction force is higher in comparison with higher wheg numbers. Greater cohesion of the medium at higher saturation levels combined with rigid wheg geometries ultimately assist robot push of force, resulting in aerial phase and increased stride length. However, aerial phase also entails greater oscillations of the robot center of mass in the Z direction (against gravity) resulting in a possible increase of cost of transport for lower wheg numbers. The final observation is consistent with the animal experiment results shown in [36] where a clear increase in stride length and velocity of the Brown Basilisk was observed between 0% and 15% but remained relatively constant between 15% and 30%. It was seen that the frequency of bipedal running remained relatively constant throughout the three saturation levels. Thus the increase of velocity at higher saturation levels was achieved by increasing stride frequency. BasiliskBot 2.0 however, has the capability of varying stride frequency by changing motor speed and varying stride length by changing leg geometry attachments. Based on Figure 3.3, for a single stride frequency and leg geometry,

effective stride length can be seen to follow a similar trend as with [36]. For instance, for a stride frequency of 20 Hz and leg geometry L5, stride length increased from approximately 30mm at 0% saturation to approximately 45mm at 15% saturation while remaining relatively constant between 15% and 30%. Overall it can be seen that for a constant range of motor frequencies tested at all three saturations, the corresponding stride lengths increased with increasing saturation level. This indicates further the effect of sinkage on dry sand and an increase in cohesion in saturated sand.

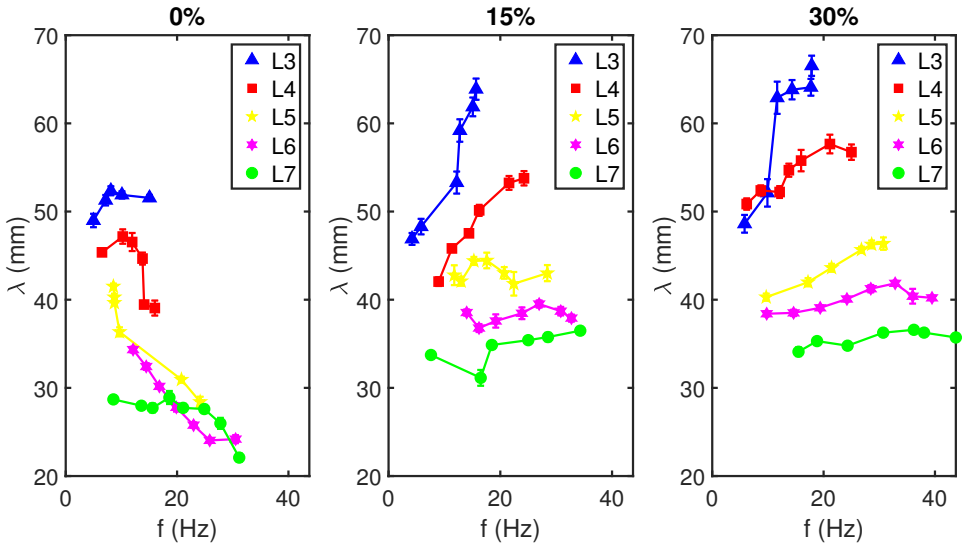

Figure 3.3: Stride length vs.stride frequency for multiple leg geometries at various saturation levels

Robot velocity vs. stride frequency (Figure 3.4) shows that maximum robot velocities achieved on saturated sand were higher in comparison with dry sand. For the tested set of saturations, robot velocity was lowest at a saturation level of 0% and highest at 30%. At each saturation level, velocity increased with increasing stride frequency. A closer look at the velocity values at 0% show a sub-linear increase in velocity with increasing stride frequencies once again exhibiting the effect of sinkage and slippage on dry sand. The gradient $\lambda = \frac{v}{f}$ tends to decrease with increasing stride frequency confirming the decrease in stride length as shown in Figure 3.3. Further-

more, for the tested experimental scenarios, maximum velocities at 0% was achieved with L3, at 15% with L4 and at 30% with L6 indicating varying stride lengths depending on the locomotion medium can be beneficial in terms of achieving desired velocities.

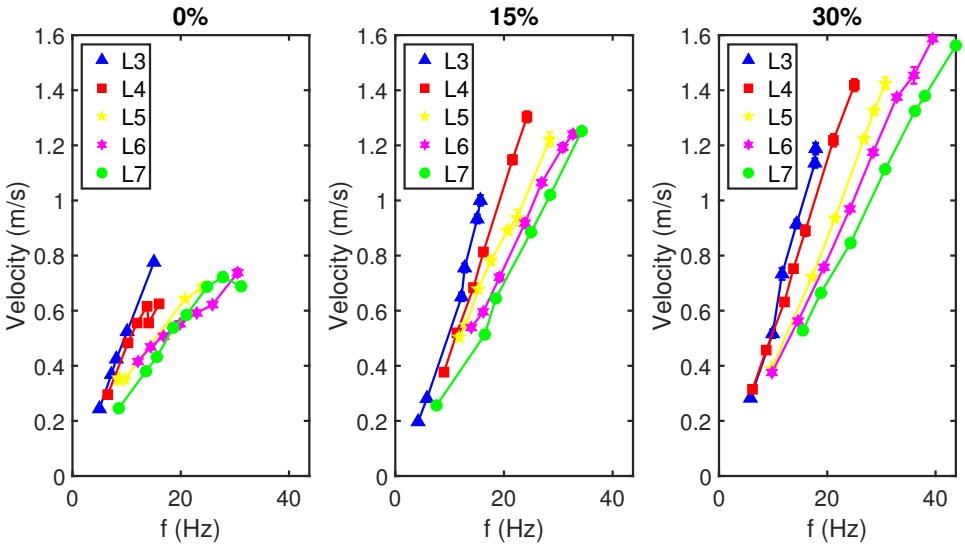

Figure 3.4: Robot velocity vs. stride frequency for multiple leg geometries at various saturation levels

Robot cost of transport vs. stride frequency for the above robot experiments are shown in Figure 3.5 from which the following conclusions could be made: (1) as frequency increased cost of transport decreased, (2) generally cost of transport decreased with increasing saturation levels, and (3) at lower frequencies cost of transport increased with decreasing wheg numbers while at higher frequencies generally the opposite held true. Cost of transport for lower wheg numbers (i.e.L3) reduced drastically when frequency was increased, while for higher wheg numbers the decrease was relatively gradual. The operating range of motors (140rpm - 445rpm)

Furthermore, animal experiment results demonstrated an increase in velocity at higher saturation levels was achieved with wider stride lengths as opposed to higher frequencies. In the current series of robotic experiments however, both stride length

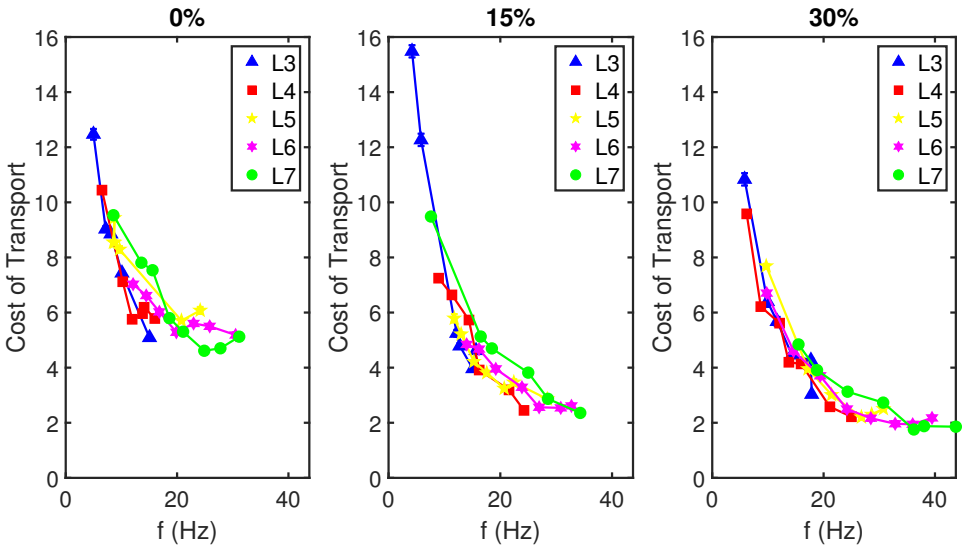

Figure 3.5: Cost of transport for multiple leg geometries at various saturation levels

and frequency were directly varied to achieve multiple velocities.

Chapter 4

QUADRUPEDAL LOCOMOTION ON DRY AND WET GRANULAR MEDIA

4.1 Overview

Althought the common Basilisk prefers bipedal locomotion for achieving higher speeds and resorts to quadrupedal locomotion for slower gait, it is beneficial to investigate the interdependence of gait parameters discussed in Chapter 3 as it pertains to quadrupedal robot motion. A primary reason for such an investigation is the potential terrestrial robotic applications. Utilizing the same experimental setup, quadrupedal robot experiments were performed in tandem with bipedal robot experiments.

4.2 Robot Experiments

Robot experiments utilized the same laboratory transition track and other experimental apparatus discussed in Chapters 1 and 3. Similar to previous experiments, the robot was powered on and once the initial offset of diagonal limbs (D1) occurred, the robot was placed at the near end of the track. Due to its alternating diagonal gait, BasiliskBot 2.0 is not statically balanced once offset has taken place. Similar to bipedal experiments, to counter robot imbalance, the robot was supported by hand while at rest to ensure only one alternating diagonal (D1) was in contact with sand. Thereafter, experiments were performed and relevant data were recorded using methods identical to the ones described in Section 3.2.2. Corresponding robot data was analyzed using the methods described in Section 3.3 to produce results similar to those discussed in Section 3.4.

4.3 Results

Similar to Section 3.4, the following plots were generated to show the effects of gait parameters on robot performance over multiple saturation levels. Figure 4.1 shows the the relationship between stride length and stride frequency, from which several observations can be made. (1) Similar to bipedal motion, stride length decreases as wheg number increases, (2) Generally stride length for each wheg geometry decreases as saturation increases from 0% to 15% but increases or remains constant between 15% and 30% saturation levels, (3) at 0% saturation, stride length decreases as stride frequency increases while while at 15% and 30% stride lengths increase with increasing stride frequency. The first observation is again a result of the rigid wheg geometries and is quite obvious. Wider gaps between spokes entail longer strides while shorter gaps entail shorter strides. However, it can be noted that the stride lengths for each wheg geometry during quadrupedal motion at 0% saturation has increased in comparison with bipedal motion (Figure 3.3). During quadrupedal gait, the presence of two points of contact as opposed to one point of contact such as the case in bipedal gait can be attributed to this increase. With two points of contact the wheg-sand contact area increases resulting in a decrease of distributed contact load per each wheg. Therefore the effect of sinkage and slippage on stride length during quadrupedal robot motion is limited and is evident when observing Figure 4.1. The second observation can be attributed to the presence of aerial phase at 15% and 30% saturation levels. During high-speed video analysis, it was observed that aerial phase impacted the performance of the robot at higher saturations due to increased media cohesion. The final observation can be attributed to properties of the granular substrates. On dry sand it can be seen that the general trend of effective stride length decreases with increasing stride frequency, which can be explained using

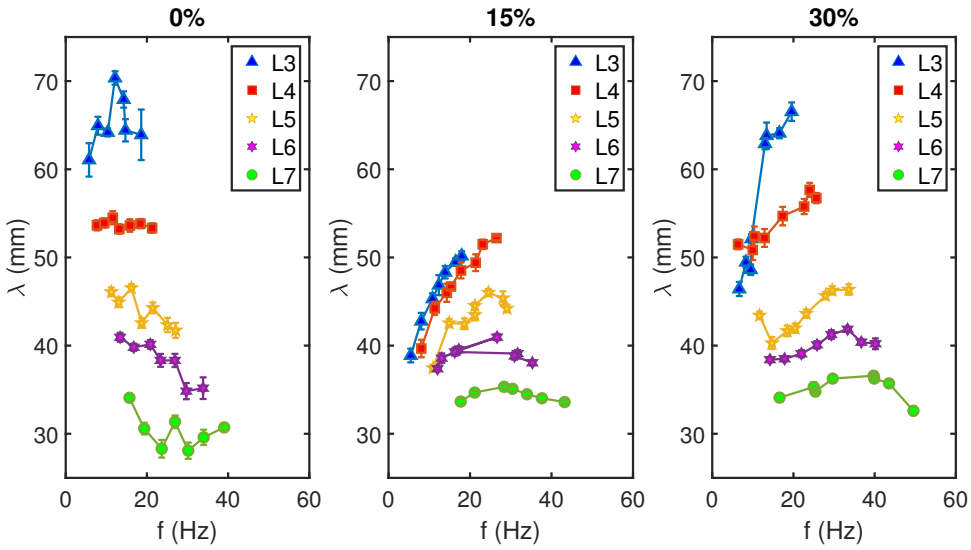

Figure 4.1: Effective stride length vs. stride frequency during quadrupedal robot locomotion at 0, 15, and 30% saturation.

the terradynamic principles described in [23]. With increasing stride frequency, sub-linear decrease in speed is expected which coincides with an equivalent decrease in stride length. Although a swimming phase is not achieved here, which would result in near-zero values for stride length, a gradual decrease is seen. At higher saturation levels, the opposite can be observed: stride length increases with increasing stride frequency. Again, increased cohesion of the medium caused by the addition of water promotes aerial phase which can be especially prevalent at higher motor frequencies.

Figure 4.2 shows the relationship between robot velocity and stride frequency. The overall effect of media saturation on robot velocity can be seen as velocity increases as saturation values increase from 0% to 30%. For instance, maximum robot velocity for a stride frequency of 40Hz for L7 on 0%, 15% and 30% saturation levels, is approximately 1.2, 1.4 and $1.6ms^{-1}$ respectively. On dry sand, a maximum velocity of approximately $1.2ms^{-1}$ is achieved with each leg geometry. With a lower spoked wheg such as L3, this velocity can be achieved at a lower frequency as opposed to a higher spoked wheg such as L7, which can be validated with $v = f\lambda$. The same trend

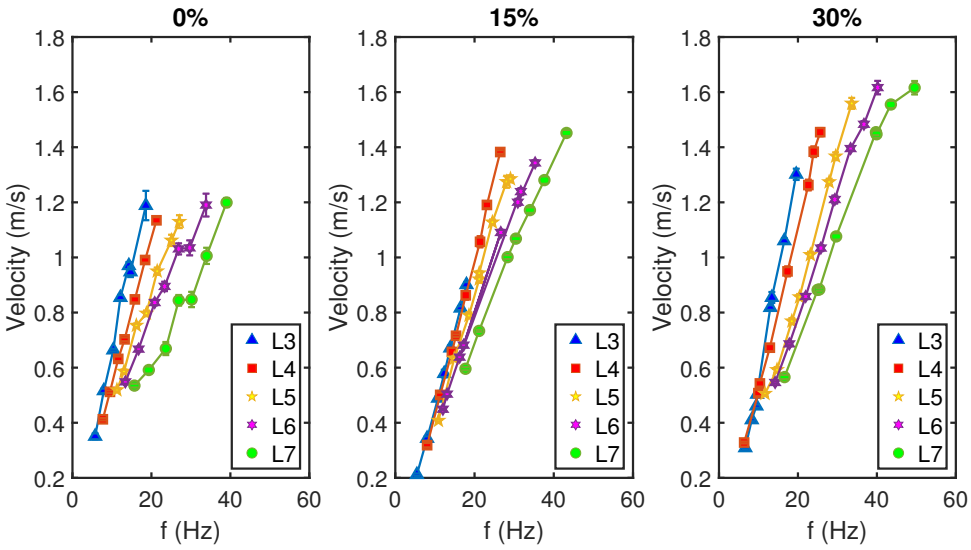

Figure 4.2: Robot velocity vs. stride frequency during quadrupedal robot locomotion at 0, 15, and 30% saturation.

is similarly observed for all leg geometries on all saturation levels.

Similar to the analysis in Chapter 3, robot energetics were determined by calculating cost of transport associated with each experimental condition. Figure 4.3 shows the relationship between cost of transport and stride frequency from which several observations can be made. (1) Cost of transport deceases with increasing stride frequency for all saturation levels. (2) The decrease in cost of transport for higher spoked whegs is more gradual compared to lower numbered whegs. (3) Cost of transport during quadrupedal motion is lower than the cost of transport values obtained during bipedal locomotion. This observation is especially evident on dry sand. The comparison of cost of transport for both modes of locomotion is also consistent with the findings of [37] which proposes that the energetics of bipedal locomotion may be higher in comparison with quadrupedal locomotion.

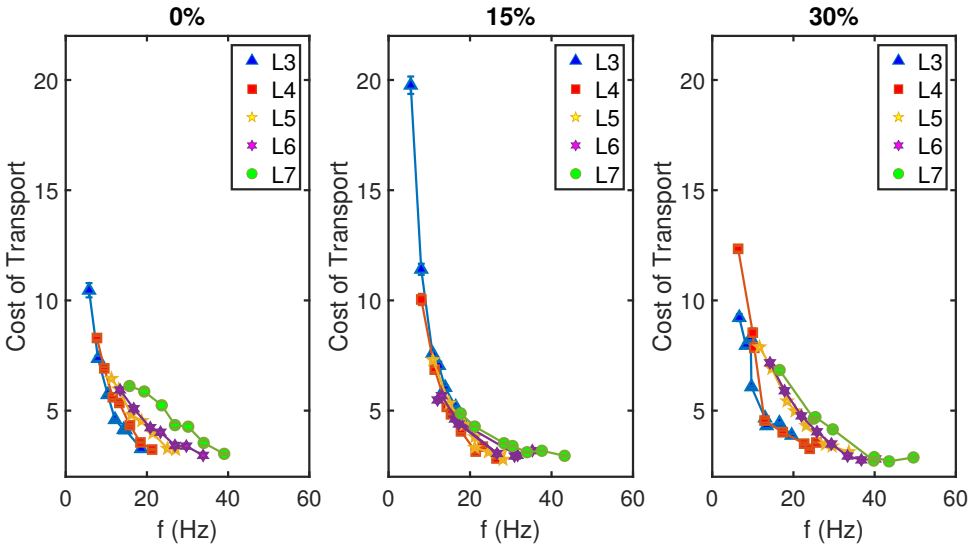

Figure 4.3: Cost of transport vs. stride frequency during quadrupedal robot locomotion at 0, 15, and 30% saturation.

Chapter 5

BASILISK TRANSITION METHODS FROM GRANULAR TO AQUATIC MEDIA

5.1 Overview

Following robot experiments on granular media, the next step of the study focused on investigating methods exhibited by the common Basilisk when transitioning from a granular surface to an aquatic media. The objectives of the study included determining preferred transition methods, determining modes of aquatic locomotion and their effectiveness, and to lay preliminary experimental groundwork for a future study aimed at determining the hydrodynamic forces acting on a Basilisk during aquatic locomotion. Two types of Basilisk species were considered for this study: Green Basilisk (*Basiliscus plumifrons*) and the Brown Basilisk (*Basiliscus vittatus*). Both species exhibit a unique ability to both run on the surface of water and swim underwater. However, as expected Green Basilisks in particular performed better in an aquatic environment, as opposed to their counterparts.

5.2 Materials and Methods

5.2.1 Animals

Four green Basilisk lizards (plumed) and three brown Basilisk lizards, obtained from an outside vendor (BackwaterReptiles), were selected for the animal locomotion experiments described in the following sections. Under Arizona State University's Institutional Animal Care and Use Committee (IACUC) protocol number 16-1504R RFC 2, the animals were housed in a vivarium facility and separately placed in aquaria

Subject	M (g)	SVL (mm)	Statistics
Green 1 (G1)	22.8	93.11	
Green 2 (G2)	20.6	92.78	
Green 3 (G3)	4.8	56.22	$\sigma_M = 13.60$
Green 4 (G4)	43.1	108.53	$\sigma_{SVL} = 19.24$
Brown 1 (B1)	17.0	84.40	
Brown 2 (B2)	16.6	86.87	$\sigma_M = 0.96$
Brown 3 (B3)	18.8	91.88	$\sigma_{SVL} = 3.11$

Table 5.1: Key physical characteristics of the test subjects used: mass and snout-to-vent length (SVL)

according to gender and other species-specific constraints to prevent breeding or any form of conflict. The artificial habitat was maintained at an average temperature of 86^oF during the day and were fed crickets as well as other dietary supplements. Mass (M) and snout-to-vent length (SVL) of each animal were measured to determine the growth of the lizards. The measured physical traits of the animals at the point of the study are given in Table 5.1

5.2.2 Experimental Setup

The transition track introduced in Chapter 1 was again used for conducting animal transition experiments. The track was modified to recreate a typical naturally occurring stream consisting of an aquatic section sandwiched by two granular terrains on either side. A side-on schematic view of the modified experimental setup is shown in Figure 5.1. In order to create three separate terrains, two 10cm high dividers were setup at 2m and 0.5m away from A and B ends of the track respectively. Dividers were sealed on both sides by applying Silicone sealant to prevent any leakage of water into the granular sections. The 2m and 0.5m sections at each end of the track were then

filled with sieved dry sand with particle sizes ranging of from $250\mu m$ to $600\mu m$ until a height of $\approx$ 10cm was reached. Water was added to the 3.5m long middle section, up to the height of the divider, to create the third substrate for lizard locomotion. A submersible water heater was placed in water to raise the average temperature to a range of $78.1 - 83.7^oF$. As an additional component of the set up, a modular ramp was installed at the base of divider 1 to create inclined or declined transitions. The adjustable ramp is capable of making 10^o increments in both positive and negative directions in a range of 90^o. For this particular study however, the ramp was kept horizontal and flush with the surface of water, i.e. at a constant angle of 0^o.

The Optitrack motion capturing system introduced in Chapter 1 was angled to envelop a capture area with length 1m - 1.5m on either side of divider 1(Figure 5.2(B)) with maximum image overlap at the divider. Camera settings of 120 frames-per-second, exposure of 30 and threshold of 255 were used for all recordings. All cameras were operated at maximum frame rate due to the speeds at which Basilisks were prone to run. Exposure and threshold settings were selected through trial and error depending on the visibility of markers in both sand and water. An Edgertonic SC1 high-speed camera was setup on the side to capture high-speed images at 1000 frames-per-second of lizard locomotion on sand, water and during transition from sand to water.

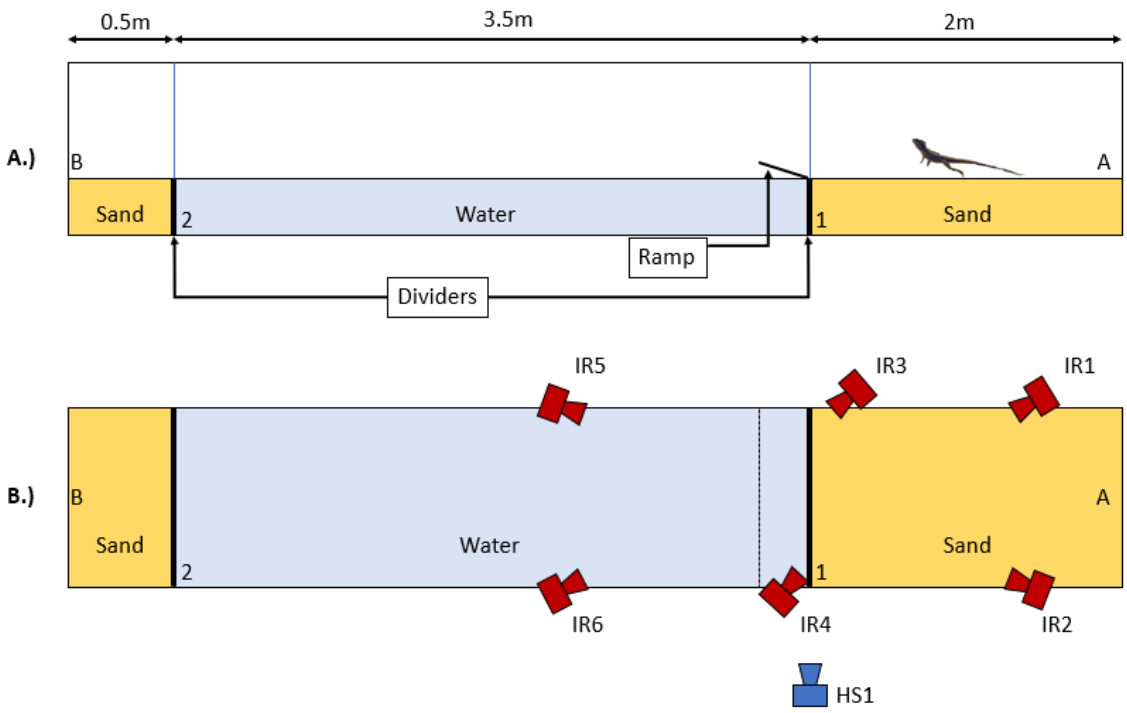

Figure 5.1: (A) Side-view of the experimental setup. Mechanical dividers, placed at 2m and 0.5m from each end separate alternating sections of sand and water. (B) Top-view of the experimental setup showing the arrangements of Optitrack Flex 13 Infrared (IR) cameras 1 through 6 and the Edgertronic SC1 high-speed camera (HS1).

5.2.3 Experimental Protocol

Experiments discussed in this section were performed over several weeks to provide sufficient rest periods for animal subjects and due to limited repeatability. Each daily set of experiments involved the use of four randomly selected lizards out of a possible seven: four green Basilisks (G1, G2, G3 and G4) and three brown Basilisks (B1, B2 and B3). Prior to experiments, the selected lizards were removed from their aquaria, put into breathable mesh containers and brought to the laboratory and placed in a humidifier (ExoTerra) set to 86^oF. Three 9mm diameter IR reflective markers were then glued to the skin of the lizards using a tissue adhesive at three different locations similar to those shown in Figure 5.2(A): the head (H), center of mass (COM) and pelvis (P). To preserve the reflectivity of the IR markers during contact with water,

each marker was sealed with clear plastic wrap.

The number of IR markers as well as the size of each marker placed on the lizard for motion tracking were dependent upon the following factors: the size and mass of the lizards, mass of each marker relative to the lizards and reflectivity of markers when submerged in water. The main constraint which dictated the selection and attachment of IR markers was the average size of the lizards being tracked. A smaller sized animal dictated the attached markers to be small and light enough to reduce as much as possible, any interference with the animal's natural motion and behavior. During preliminary tests it was observed that when the lizard interacted with water, via either running or swimming, continuous tracking of all three markers became increasingly difficult as marker size decreased. The passive nature of the markers and insufficient combined reflective surface were cited as the main reasons for this restriction. Through trial and error, 9mm markers were determined to be the ideal

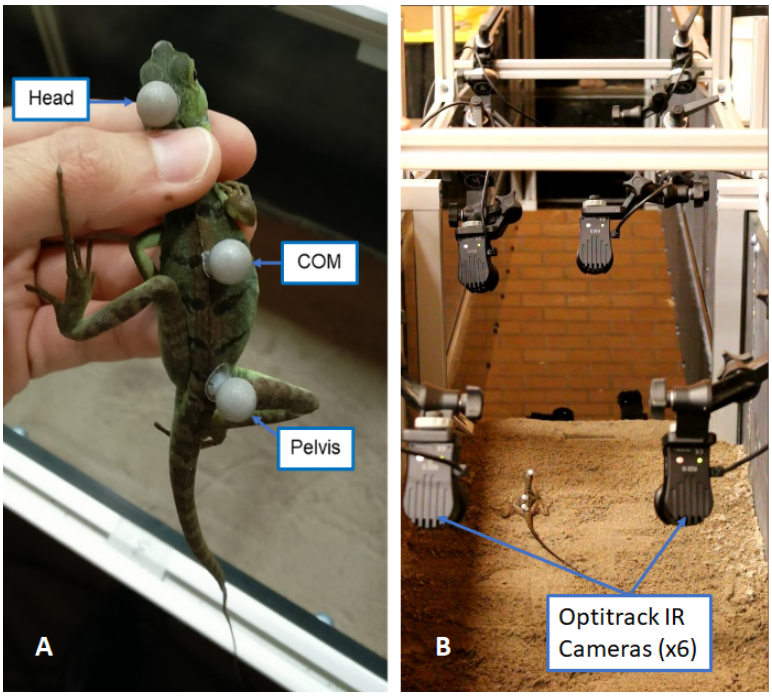

Figure 5.2: A schematic diagram of the experimental setup in the custom built transition track.

marker size to be used for successful continuous data acquisition. The mass of each 9mm IR reflective marker used is 0.31g and is 1.4% of the average mass of the green Basilisk and 1.7% of the brown Basilisk used for the current study. Thus, for a combination of 3 markers, the relative mass is 4.2% and 5.1% respectively. Although for the juvenile green Basilisk (G3), the three markers amount to 19.3% of its own body mass, the effect of marker-added mass on the overall locomotion characteristics of the lizards were assumed to be minimal.

Once all three H, COM and P markers were securely attached to the lizard, it was immediately placed down on the sand closer to 'A' end of the track as shown in Figure 5.1 while Optitrack cameras continuously recorded data. Special attention was given to minimize the time the lizard spent in the hands of the animal handler and initially on sand. External objects such as props made of bird feathers and the mesh bags in which lizards were temporarily transported were used to simulate predatory movements to ultimately promote the animals to run. Once the lizard completed its run from one end of the track to the other, IR data recording was paused and the lizard was removed from the track and placed back in the humidifier for a rest period of 30 minutes. This process was repeated for the remaining animals in the sequence. Due to limited repeatability caused by the animal's physiological factors, a maximum of three trials per animal were conducted on a single day.

5.2.4 Data Acquisition

Six Optitrack Flex 13 cameras arranged in the manner shown in Figure 5.1(B) with settings denoted in Section 5.2.2, continuously tracked the lizards motion along the transition track by tracking H, COM and P markers. Motive 1.10, Optitrack's motion capturing software, enabled data acquisition, real time viewing of the lizard's motion as well as basic post-processing. Once each run was complete, each take

was manually verified through visual inspection to determine if continuous tracking of all three markers took place. Basic post-processing tools of the software enabled simple reconstruction (stitching) of takes through interpolation. Stitching became especially useful when determining the motion of the lizards on and under water, as interference seemed to be more present over the surface of water. Upon successful visual inspection, each data file was saved in a CSV format for post-processing and analysis. The exported data files consisted of camera settings, time-stamp and x,y and z coordinates of H, COM and P markers with respect to the calibration reference frame.

In addition to the quantitative data given by the Optitrack system, high-speed videos were recorded using an Edgertonic SC1 high-speed camera (HS1) as shown in Figure 5.1(B). Each recording was performed at 1000fps and captured qualitative data relating to transition and was ultimately used to visually inspect macro level motions of the lizard as it transitions from sand to water.

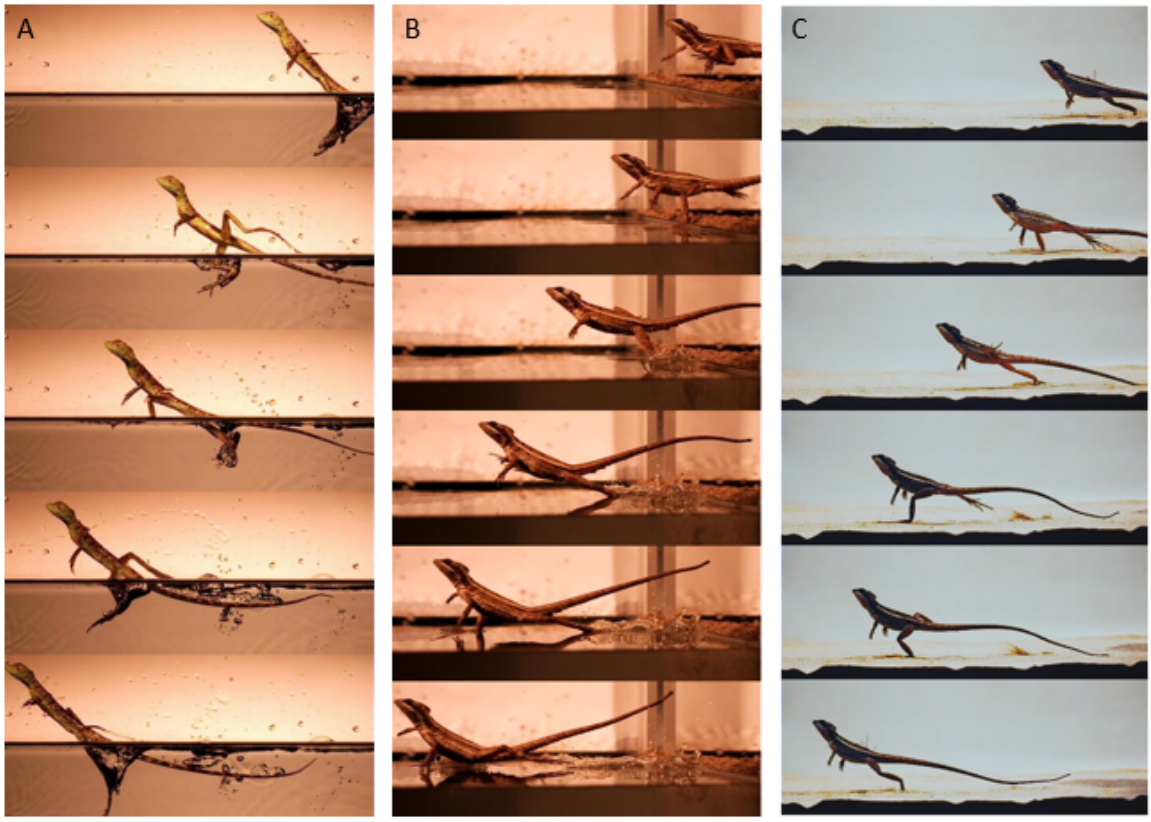

Figure 5.3: Basilisk lizards are known for their multi-terrain locomotion capabilities and in particular their unique ability to run on the surface of water. In many instances of running, bipedal running is observed where high speeds are required. Using the Edgertronic SC1 high-speed camera to record side-on motion of lizards qualitative information regarding styles of motion were collected. (A) A juvenile green Basilisk running on water. (B) Adult brown Basilisk transitioning from sand to water. (C) Adult brown Basilisk running on sand.

5.3 Data Analysis

A combination of visual observation and software enabled post-processing was used to determine the locomotion characteristics of Basilisk lizards during motion in water and in transition. Basic post-processing of tracking data such as labeling, stitching and removing artifacts were performed in Motive 1.10. After which, the relevant data was imported into MATLAB to determine select physical characteristics of locomotion.

Due to limitations in the frame rate of the Optitrack recording system and the

intermittent interference caused by water during high-speed lizard motion, continuous tracking of the passive IR markers was not always ensured. Therefore in several instances the system recorded discrete segments of IR marker data corresponding to H, COM and P makers with narrow gaps of varying length, corresponding to null data, separating these data segments. Thus, the first step in analyzing data was to convert these discrete segments into continuous streams of data through stitching. Analyzing marker trajectories in Motive with respect to the system defined coordinated system suggested that the motion of H, COM and P markers followed patterns of undulation and therefore close approximation of segments of null data could be achieved using multiple methods of interpolation. In addition, as multiple cameras were used to maximize image overlap, the gaps in data were seen to be narrow and thus the error introduced by interpolation was assumed to be minimal. Using Motive 1.10, cubic interpolation was performed to convert the discrete segments of data into continuous streams of data.

The corresponding tracking data files containing time based x, y and z locations of H, COM and P markers were then exported from Motive 1.10 into a MATLAB environment for further analysis. With the simplified three dimensional kinematic model shown in Figure 5.4 as a basis, the recorded tracking data and their corresponding time-stamps were used to calculate locomotion characteristics such as body position, body orientation and forward velocity of center of mass. For a particular maker M denoted by $\vec{r}_M = r_x\hat{\mathbf{i}} + r_y\hat{\mathbf{j}} + r_z\hat{\mathbf{k}}$, its velocities in each principle direction can be calculated as shown below using (5.1) and (5.2) and absolute marker velocity $|V_M|$, using 5.3.

$$\vec{v_n} = \frac{d\vec{r_n}}{dt}; \qquad n = i, j, k \tag{5.1}$$

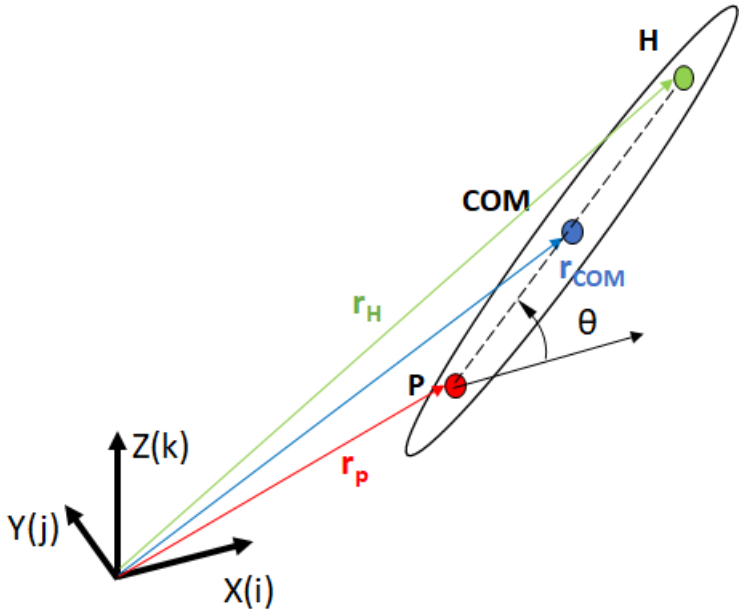

Figure 5.4: Kinematics of lizard motion. Three markers attached to the head (H), center of mass (COM) and pelvis (P) provide coordinates of lizard body in a user defined reference frame. Body pitch (θ) is the inclination of $\vec{r}_{PH}$ to the XY plane.

$$\vec{v}_n = \frac{\vec{r}_n(t+\Delta t) - \vec{r}_n(t)}{\Delta t}; \qquad n = i, j, k \tag{5.2}$$

$$|V_M| = \sqrt{v_{\hat{i}}^2 + v_{\hat{j}}^2 + v_{\hat{k}}^2} \tag{5.3}$$

$$\vec{r}_{PH} = r_{PH,X}\hat{\mathbf{i}} + r_{PH,Y}\hat{\mathbf{j}} + r_{PH,Z}\hat{\mathbf{k}} \tag{5.4}$$

$$\theta = tan^{-1}\left[\frac{r_{PH,Z}}{\sqrt{r_{PH,X}^2 + r_{PH,Y}^2}}\right] \tag{5.5}$$

Applying equations (5.1) - (5.3) $|V_H|$, $|V_{COM}|$ and $|V_P|$ were calculated for H,COM and P markers respectively for each successful animal trial. The main parameter in determining body orientation studied here is body pitch. With reference to Figure 5.4, pitch (θ) of the lizard's body is defined in this text as the inclination of the vector

$\vec{r}_{PH} = \vec{r}_H - \vec{r}_P$ to the XY plane. Thus, for the given vector $\vec{r}_{PH}$, its instantaneous pitch is given by equation (5.5). Each parameter noted above, was calculated for every successful trial and the relevant values were used to quantitatively compare and categorize animal motion.

Figure 5.5: Representative top-view of a Brown basilisk lizard swimming underwater exhibiting undulation.

5.4 Results

Based on analyzed tracking data, video recordings and real-time visual observations, methods of transition and locomotion in water were put into the following categories. Transitioning from land to water was mainly done via two different methods which were jumping (J) from either the platform or sand into the water, and diving (D). Jumping was considered to be a clear and active use of the lizard's limbs to

gain a vertical displacement exceeding twice the vertical distance between the lizard's center of mass and the substrate while at rest. In contrast, diving was considered to be a smoother transition keeping the center of mass lower and not exceeding the above mentioned vertical limit. Locomotion on water was also categorized into two main methods which were running (R) and swimming (S). It was observed that for one complete trial, the lizards used one of the two methods of transition, and either a single method or a combination of water locomotion methods.

It was observed that for all combined Brown and Green Basilisk experiments, during 71.4% of the trials the lizards used jumping as their method of transition, while 28.6% of the trials saw diving. Thereafter in terms of in-water locomotion, 46.4% of the trials saw lizards running on water while 53.6% resulted in swimming.

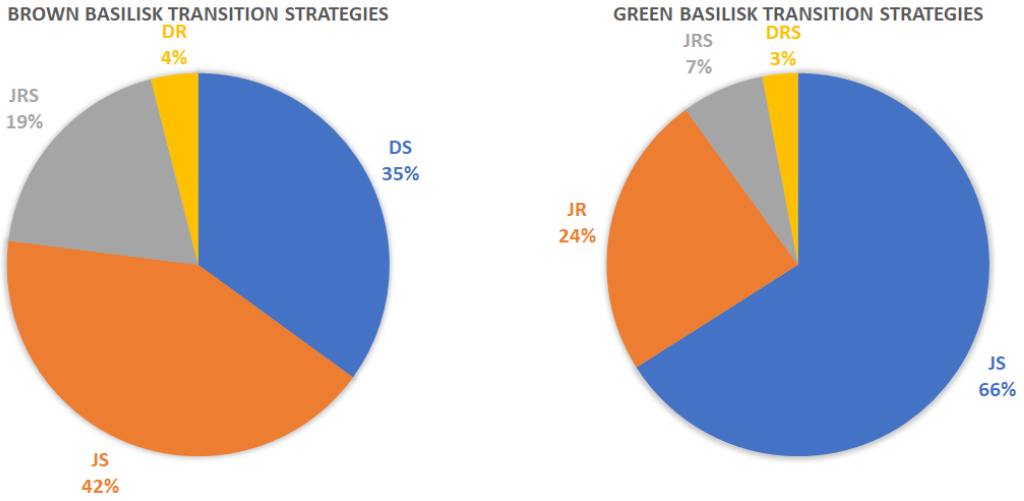

Figure 5.6: Common transition strategies used by Brown and Green Basilisk Lizards

Transition and locomotion strategies used by both Brown and Green Basilisks are shown in Figure 5.6. Both brown and green species of Basilisk lizards exhibited permutations of the above mentioned transition and locomotion methods. The main permutations depicted in the above data is: jumping-swimming (JS), jumping-running (JR), jumping-running-swimming (JRS), diving-swimming (DS), diving-running (DR) and

diving-running-swimming (DRS).

Several conclusions can be made from the above data. (1) Both Brown and Green species of Basilisk exhibited an affinity for jumping and swimming. Looking at Figure 5.6 it can be seen that for 42% of brown and 66% of green Basilisk trials, the animals chose jumping and swimming. (2) In general for both species of Basilisk, swimming appeared to be the most common method of in-water locomotion shown, as opposed to running. 96% of the trials conducted for brown Basilisks saw some form of swimming in combination with either mode of transition and in-water locomotion. These methods were jumping-swimming, diving-swimming and jumping-running-swimming in order. A combined 76% of green Basilisk lizard trials used swimming for in-water locomotion comprising of jumping-swimming, jumping-running-swimming and diving-running-swimming. (3) Green Basilisks were more prone to running on water in comparison with Brown Basilisks. Green Basilisks used running either fully or partially for 34% of the trials in the form of: jumping-running, jumping-running-swimming, and diving-running-swimming while brown species used running for 23% of the time in the form of jumping-running-swimming and diving-running.

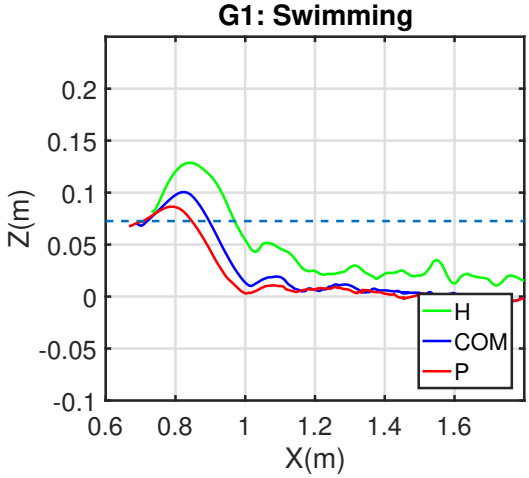

Figure 5.7: The path of H, COM and P markers in the XZ plane for a green Basilisk (G1) engaging in jumping-swimming

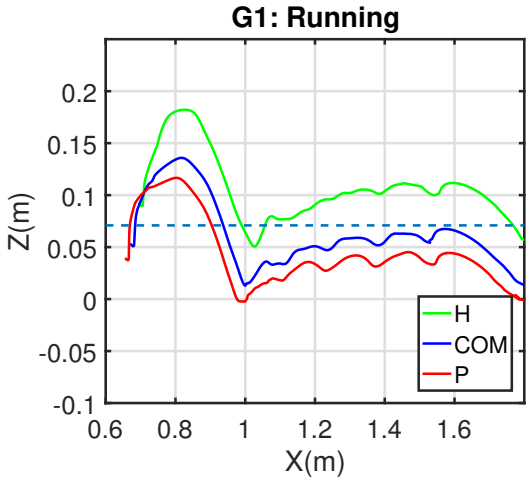

Figure 5.8: The path of H, COM and P markers in the XZ plane for a green Basilisk (G1) engaging in jumping-running

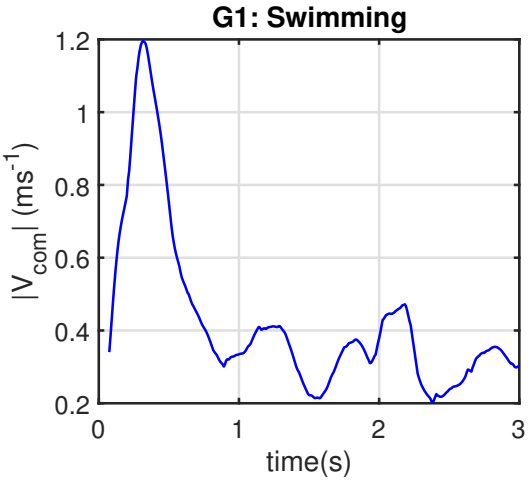

Figure 5.9: Absolute velocity of COM in the XZ plane for a green Basilisk (G1) engaging in jumping-swimming

Figures 5.7 and 5.8 show the typical path of H, COM and P markers in the XZ plane for a green basilisk, engaged in swimming and running, along a straight path. In both instances, the animal can be seen jumping from its initial point on the ramp and land in the water following with either swimming and running. In the case of swimming, all three markers are below the surface of water denoted by the dashed line indicating that once the lizard landed in water, underwater locomotion was performed. Furthermore it can be seen that in comparison with running, the

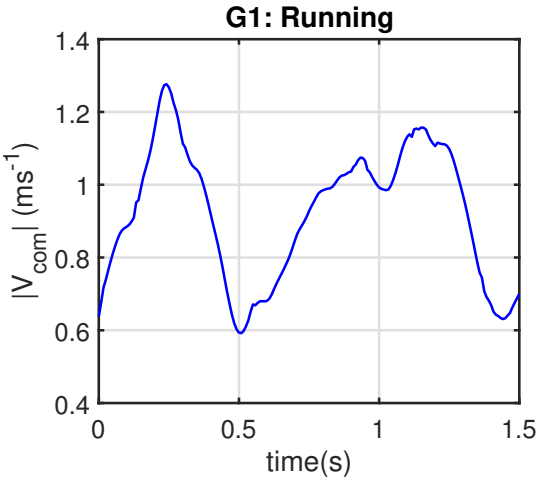

Figure 5.10: Absolute velocity of COM in the XZ plane for a green Basilisk (G1) engaging in jumping-running in a straight path.

vertical band between markers H and P are much narrower, indicating a low pitch angle while swimming. As expected a lower pitch angle results in a reduced cross-sectional area culminating in reduced effects of hydrodynamic drag. In the case of running, the gaps between H, COM and P markers are wider confirming the green Basilisk's increased near-vertical pitch angle, allowing for a more balanced bipedal running. The corresponding absolute COM velocities for the instances given above, are shown below in Figures 5.9 and 5.10, respectively. In both cases, a velocity spike can be observed at the beginning of the trial caused by jumping. In the case of swimming, the lizard appears to achieve a steady state after the rapid velocity spike. In contrast, velocity of COM during running is significantly higher and continues to increase up to a maximum of almost four times the average swimming velocity.

Chapter 6

CONCLUSION AND FUTURE RESEARCH

6.1 Conclusion

Several conclusions can be made from the research presented in this thesis. The systematic use of a bio-inspired robot with physical characteristics similar to the model organism, provided significant quantitative and qualitative information relating to investigated locomotion characteristics. Studies also revealed physiological limitations of model organisms which can be accounted for with proper robotic locomotor design. Higher saturation of granular media favored legged locomotion caused by increased substrate cohesion. An increase in saturation caused an increase of velocity caused by greater stride length. Energetics of robotic locomotion over dry and wet granular media appeared to be consistent with gait patterns exhibited by the *Basiliscus* over similar substrates. The *Basilisk's* preference of gait patterns of gait parameters can therefore be understood in terms of energetics.

Preliminary animal experiments revealed animal preferences for transitioning from granular to aquatic media. All test subjects showed tremendous capability to run on water as well as swim in water at high velocities. The *Basiliscus plumifrons* in particular exhibited greater preference and aptitude for running on water. Passive and active morphological features of animal test subjects which aided on-water locomotion was observed and was determined to be consistent with previous observations.

6.2 Future Research

Following the overall research objectives highlighted in Chapter 1, the next step towards designing a Basilisk inspired robotic locomotor is to determine and model the kinetics of animal-water interactions. Such a model will in turn provide a useful base for designing an aquatic locomotor. A feasible next step is to design and build an experimental setup to characterize a basilisk running on water and determine the hydro-dynamic forces during on-water running. Results obtained through experiments can then be used to design leg appendages to enable on-water robot locomotion. The simple passive morphological features of the Basilisk, observed during experiments can be recreated artificially and incorporated into various leg appendages. Multiple existing robotic platforms can be utilized for systematic experiments.

REFERENCES

[1] D J Irschick and B C Jayne. High-speed lizard locomotion. page 19.

[2] Richard C. Snyder. Adaptations for Bipedal Locomotion of Lizards. *American Zoologist*, 2(2):191–203, 1962.

[3] Milton Hildebrand. Motions of the Running Cheetah and Horse. *Journal of Mammalogy*, 40(4):481–495, 1959.

[4] Virginia C. Maiorana. Tail autotomy, functional conflicts and their resolution by a salamander. *Nature*, 265(5594):533–535, February 1977.

[5] J. D. Congdon, L. J. Vitt, and W. W. King. Geckos: Adaptive Significance and Energetics of Tail Autotomy. *Science*, 184(4144):1379–1380, June 1974.

[6] Christopher B. Daniels. Running: An Escape Strategy Enhanced by Autotomy. *Herpetologica*, 39(2):162–165, 1983.

[7] Fred Punzo. Tail Autotomy and Running Speed in the Lizards Cophosaurus texanus and Uma notata. *Journal of Herpetology*, 16(3):329–331, 1982.

[8] Royce E. Ballinger, Joseph W. Nietfeldt, and James J. Krupa. An Experimental Analysis of the Role of the Tail in Attaining High Running Speed in Cnemidophorus sexlineatus (Reptilia: Squamata: Lacertilia). *Herpetologica*, 35(2):114–116, 1979.

[9] Theodore Garland and Christine M. Janis. Does metatarsal/femur ratio predict maximal running speed in cursorial mammals? *Journal of Zoology*, 229(1):133–151, January 1993.

[10] Peter C. Wainwright and Stephen M. Reilly. *Ecological Morphology: Integrative Organismal Biology*. University of Chicago Press, August 1994. Google-Books-ID: gsvD8es6L2gC.

[11] Joshua Laerm. A Functional Analysis of Morphological Variation and Differential Niche Utilization in Basilisk Lizards. *Ecology*, 55(2):404–411, 1974.

[12] Jonathan A. Campbell. *Amphibians and Reptiles of Northern Guatemala, the Yucatan, and Belize*. University of Oklahoma Press, February 1999. Google-Books-ID: orUl8Ezs1iQC.

[13] Green Basilisk Lizard | National Geographic, April 2010.

[14] S. Tonia Hsieh. Three-dimensional hindlimb kinematics of water running in the plumed basilisk lizard (Basiliscus plumifrons). *Journal of Experimental Biology*, 206(23):4363–4377, December 2003.

[15] Richard C. Snyder. Bipedal Locomotion of the Lizard Basiliscus basiliscus. *Copeia*, 1949(2):129–137, 1949.

[16] C. Li, S. T. Hsieh, and D. I. Goldman. Multi-functional foot use during running in the zebra-tailed lizard (Callisaurus draconoides). *Journal of Experimental Biology*, 215(18):3293–3308, September 2012.

[17] Joshua Laerm. Aquatic Bipedalism in the Basilisk Lizard: The Analysis of an Adaptive Strategy. *The American Midland Naturalist*, 89(2):314–333, 1973.

[18] Harold F. Hirth. The Ecology of Two Lizards on a Tropical Beach. *Ecological Monographs*, 33(2):83–112, 1963.

[19] A. Stanley Rand and Hymen Marx. Running Speed of the Lizard Basiliscus basiliscus on Water. *Copeia*, 1967(1):230–233, 1967.

[20] T. M. Lejeune, P. A. Willems, and N. C. Heglund. Mechanics and energetics of human locomotion on sand. *Journal of Experimental Biology*, 201(13):2071–2080, July 1998.

[21] R. Brandt, F. Galvani, and T. Kohlsdorf. Sprint performance of a generalist lizard running on different substrates: grip matters. *Journal of Zoology*, 297(1):15–21, September 2015.

[22] J. Glasheen and T. Mcmahon. Size-dependence of water-running ability in basilisk lizards (Basiliscus basiliscus). *Journal of Experimental Biology*, 199(12):2611–2618, December 1996.

[23] C. Li, P. B. Umbanhowar, H. Komsuoglu, D. E. Koditschek, and D. I. Goldman. Sensitive dependence of the motion of a legged robot on granular media. *Proceedings of the National Academy of Sciences*, 106(9):3029–3034, March 2009.

[24] Uluc Saranli, Martin Buehler, and Daniel E. Koditschek. RHex: A Simple and Highly Mobile Hexapod Robot. *The International Journal of Robotics Research*, 20(7):616–631, July 2001.

[25] Kevin C Galloway, Galen Clark Haynes, B Deniz Ilhan, Aaron M Johnson, Ryan Knopf, Goran A Lynch, Benjamin N Plotnick, Mackenzie White, and Daniel E Koditschek. X-RHex: A Highly Mobile Hexapedal Robot for Sensorimotor Tasks. page 35.

[26] Robert T. Schroer, Matthew J. Boggess, Richard J. Bachmann, Roger D. Quinn, and Roy E. Ritzmann. Comparing cockroach and whegs robot body motion. In *in: Proceedings of the IEEE International Conference on Robotics and Automation, April 2004*, pages 3288–3293, 2004.

[27] N Neville and M Buehler. Towards bipedal running of a six-legged robot. page 8.

[28] Daniel E. Koditschek, Robert J. Full, and Martin Buehler. Mechanical aspects of legged locomotion control. *Arthropod Structure & Development*, 33(3):251–272, July 2004.

[29] Sangbae Kim, Jonathan E. Clark, and Mark R. Cutkosky. iSprawl: Design and Tuning for High-speed Autonomous Open-loop Running. *The International Journal of Robotics Research*, 25(9):903–912, September 2006.

[30] Warren W. Dickinson and John D. Ward. Low depositional porosity in eolian sands and sandstones, Namib Desert. *Journal of Sedimentary Research*, 64(2a):226–232, April 1994.

[31] Yang Ding, Nick Gravish, and Daniel I. Goldman. Drag Induced Lift in Granular Media. *Physical Review Letters*, 106(2):028001, January 2011.

[32] A Terradynamics of Legged Locomotion on Granular Media | Science.

[33] Feifei Qian, Tingnan Zhang, chen Li, Aaron Hoover, Pierangelo Masarati, Paul Birkmeyer, Andrew Pullin, Ronald Fearing, and Dan Goldman. Walking and running on yielding and fluidizing ground. In *Robotics: Science and Systems VIII*. Robotics: Science and Systems Foundation, July 2012.

[34] M. Scheel, R. Seemann, M. Brinkmann, M. Di Michiel, A. Sheppard, and S. Herminghaus. Liquid distribution and cohesion in wet granular assemblies beyond the capillary bridge regime. *Journal of Physics: Condensed Matter*, 20(49):494236, 2008.

[35] M. Scheel, R. Seemann, M. Brinkmann, M. Di Michiel, A. Sheppard, B. Breidenbach, and S. Herminghaus. Morphological clues to wet granular pile stability. *Nature Materials*, 7(3):189–193, March 2008.

[36] Hosain Bagheri, Vishwarath Taduru, Sachin Panchal, Shawn White, and Hamidreza Marvi. Animal and Robotic Locomotion on Wet Granular Media. In Michael Mangan, Mark Cutkosky, Anna Mura, Paul F.M.J. Verschure, Tony Prescott, and Nathan Lepora, editors, *Biomimetic and Biohybrid Systems*, Lecture Notes in Computer Science, pages 13–24. Springer International Publishing, 2017.

[37] Thomas J Roberts, Rodger Kram, Peter G Weyand, and C Richard Taylor. ENERGETICS OF BIPEDAL RUNNING. page 7.